

1 Experimental chemical budgets of OH, HO₂ and RO₂ radicals in 2 rural air in West-Germany during the JULIAC campaign 2019

3 Changmin Cho^{1,*}, Hendrik Fuchs¹, Andreas Hofzumahaus¹, Frank Holland¹, William J. Bloss³,
4 Birger Bohn¹, Hans-Peter Dorn¹, Marvin Glowania¹, Thorsten Hohaus¹, Lu Liu¹, Paul S.
5 Monks², Doreen Niether¹, Franz Rohrer¹, Roberto Sommariva^{2,3}, Zhaofeng Tan¹, Ralf Tillmann¹,
6 Astrid Kiendler-Scharr¹, Andreas Wahner¹, and Anna Novelli¹

7 ¹Forschungszentrum Jülich, Institute of Energy and Climate Research: Troposphere (IEK-8), Jülich,
8 Germany

9 ²Department of Chemistry, University of Leicester, Leicester, UK

10 ³School of Geography, Earth and Environmental Sciences, University of Birmingham, Birmingham, UK

11 *Now at: School of Earth Sciences and Environmental Engineering, Gwangju Institute of Science and
12 Technology (GIST), Gwangju, South Korea

13 *Correspondence to:* Hendrik Fuchs (h.fuchs@fz-juelich.de) and Anna Novelli (a.novelli@fz-juelich.de)

14 **Abstract.**

15 Photochemical processes in ambient air were studied using the atmospheric simulation chamber SAPHIR
16 at Forschungszentrum Jülich, Germany. Ambient air was continuously drawn into the chamber through a
17 50 m high inlet line and passed through the chamber for one month in each season throughout 2019. The
18 residence time of the air inside the chamber was about one hour. As the research center is surrounded by a
19 mixed deciduous forest and is located close to the city Jülich, the sampled air was influenced by both
20 anthropogenic and biogenic emissions. Measurements of hydroxyl (OH), hydroperoxyl (HO₂) and organic
21 peroxy (RO₂) radicals were achieved by a laser-induced fluorescence instrument. The radical
22 measurements together with measurements of OH reactivity (k_{OH} , the inverse of the OH lifetime) and a
23 comprehensive set of trace gas concentrations and aerosol properties allowed for the investigation of the
24 seasonal and diurnal variation of radical production and destruction pathways. In spring and summer
25 periods, median OH concentrations reached $6 \times 10^6 \text{ cm}^{-3}$ at noon, and median concentrations of both, HO₂
26 and RO₂ radicals, were $3 \times 10^8 \text{ cm}^{-3}$. The measured OH reactivity was between 4 and 18 s⁻¹ in both
27 seasons. The total reaction rate of peroxy radicals with NO was found to be consistent with production
28 rates of odd oxygen ($O_X = \text{NO}_2 + \text{O}_3$) determined from NO₂ and O₃ concentration measurements. The
29 chemical budgets of radicals were analysed for the spring and summer seasons, when peroxy radical
30 concentrations were above the detection limit. For most conditions, the concentrations of radicals were
31 mainly sustained by the regeneration of OH via reactions of HO₂ and RO₂ radicals with nitric oxide (NO).
32 The median diurnal profiles of the total radical production and destruction rates showed maxima between
33 3 to 8 ppbv h⁻¹ for OH, HO₂ and RO₂. Total RO_X (OH, HO₂ and RO₂) initiation and termination rates
34 were below 3 ppbv h⁻¹. The highest OH radical turnover rate of 13 ppbv h⁻¹ was observed during a high-
35 temperature (max 40°C) period in August. In this period, the highest HO₂, RO₂ and RO_X turnover rates
36 were around 11, 10 and 4 ppbv h⁻¹, respectively. When NO mixing ratios were between 1 ppbv to 3 ppbv,
37 OH and HO₂ production and destruction rates were balanced, but unexplained RO₂ and RO_X production
38 reactions with median rates of 2 ppbv h⁻¹ and 0.4 ppbv h⁻¹, respectively, were required to balance their
39 destruction. For NO mixing ratios above 3 ppbv, the peroxy radical reaction rates with NO were highly

40 uncertain due to the low peroxy radical concentrations close to the limit of NO interferences in the HO₂
41 and RO₂ measurements. For NO mixing ratios below 1 ppbv, a missing source for OH and a missing sink
42 for HO₂ were found with maximum rates of 3.0 ppbv h⁻¹ and 2.0 ppbv h⁻¹, respectively. The missing OH
43 source consisted likely of a combination of a missing inter-radical HO₂ to OH conversion reaction (up to
44 2 ppbv h⁻¹) and a missing primary radical source (0.5 – 1.4 ppbv h⁻¹). The dataset collected in this
45 campaign allowed to analyze the potential impact of OH regeneration from RO₂ isomerization reactions
46 from isoprene, HO₂ uptake on aerosol, and RO₂ production from chlorine chemistry on radical production
47 and destruction rates. These processes were negligible for the chemical conditions encountered in this
48 study.

49 **1 Introduction**

50 The hydroxyl (OH) radical is the dominant daytime atmospheric oxidant. It reacts with most trace gases
51 in the troposphere and thereby controls the rate of their removal and chemical transformation. In the
52 lower troposphere, OH is primarily produced by solar photolysis of ozone (O₃) and nitrous acid (HONO).
53 The reaction of OH with trace gases leads to the formation of hydroperoxy (HO₂) or organic peroxy (RO₂,
54 with R = organic group) radicals, which undergo further radical reactions. Generally, these reactions are
55 cyclic chain reactions, in which OH, HO₂, and RO₂ are converted into each other, while at the same time
56 emitted pollutants are oxidized and converted into secondary pollutants such ozone and oxygenated
57 volatile organic compounds (OVOCs). Because the conversion of radicals occurs on a time scale of
58 seconds to minutes, they are often referred to as the RO_x family (OH + HO₂ + RO₂). The most important
59 radical reactions in the lower are summarized in Table 1. Understanding the radical chemistry is the basis
60 for reliable predictions of the atmospheric lifetime and chemical transformation of air pollutants and
61 climate-relevant gases by atmospheric chemistry models (Stone et al., 2012).

62 The level of agreement between simulated and observed radical concentrations in various environments
63 shows the degree of understanding of the underlying radical chemical mechanism. Even though good
64 agreement is found in some cases (Tan et al., 2001; Konrad et al., 2003; Mihelcic et al., 2003; Lelieveld et
65 al., 2008; Kubistin et al., 2010; Whalley et al., 2011), there are significant unexplained discrepancies
66 between modelled and measured OH in forested regions (Wolfe et al., 2011; Griffith et al., 2013; Kim et
67 al., 2013; Hens et al., 2014; Wolfe et al., 2014) and of HO₂ and RO₂ in polluted areas (Ren et al., 2003;
68 Ren et al., 2006; Kanaya et al., 2007; Dusanter et al., 2009; Chen et al., 2010; Ren et al., 2013; Brune et
69 al., 2016; Tan et al., 2018; Slater et al., 2020; Whalley et al., 2021), while different results are found
70 depending on the abundance of nitric oxide (NO) in rural environments (Hofzumahaus et al., 2009; Lou et
71 al., 2010; Elshorbany et al., 2012; Kanaya et al., 2012; Tan et al., 2017).

72 A chemical budget analysis using measured OH, HO₂ and RO₂ radical concentrations can help assessing
73 the strength of different radical production and loss paths. This allows to identify possible missing
74 chemical processes by comparing the total production and destruction rates for the different radicals as
75 concentrations are expected to be in steady-state due to their short chemical lifetime. A large number of
76 measurements needs to be available (e.g., OH reactivity, OH, peroxy radicals), therefore, there have been
77 only few studies focusing on the analysis of the chemical budget for OH radicals so far (Handisides et al.,
78 2003; Hofzumahaus et al., 2009; Brune et al., 2016; Whalley et al., 2018; Tan et al., 2019; Whalley et al.,
79 2021).

80 Results from field campaigns in China showed a larger OH radical destruction rate compared to its
81 production rate in the afternoon, which points to an unaccounted OH radical source. Discrepancies were
82 highest, when NO mixing ratios were lower than 2 ppbv (Hofzumahaus et al., 2009; Tan et al., 2019;
83 Whalley et al., 2021). On the other hand, studies in urban areas in California (Brune et al., 2016) and in
84 London (Whalley et al., 2018) as well as in a rural area in Hohenpeissenberg (Handisides et al., 2003)
85 showed no significant gap between the OH production and destruction rates. Recently, radical
86 measurements including RO₂ enabled the investigation of HO₂, RO₂, and RO_x production and destruction
87 rates in field campaigns in China (Tan et al., 2019; Whalley et al., 2021). Tan et al. (2019) showed that a
88 RO₂ loss process was required in a campaign in Wangdu in summer, while HO₂ production and
89 destruction rates were balanced. This suggests a missing conversion of RO₂ to OH in addition to the
90 reaction of peroxy radicals with NO. Furthermore, Whalley et al. (2021) found large imbalances between
91 peroxy radical production and destruction rates in Beijing indicating a substantially slower propagation of
92 RO₂ to HO₂ radicals than anticipated.

93 In this study, OH, HO₂, and RO₂ radical concentrations as well as OH reactivity, the inverse of the OH
94 radical lifetime, were measured in the atmospheric simulation chamber SAPHIR on campus of
95 Forschungszentrum Jülich (FZJ), Germany, in the Jülich Atmospheric Chemistry Project Campaign
96 (JULIAC). Ambient air was sampled from 50 m height into the SAPHIR chamber. From this data set, a
97 chemical budget analysis of OH, HO₂, RO₂ radicals, and their sum (RO_x) was done using measured
98 concentrations allowing to investigate, if all radical production and destruction processes were accounted
99 for during spring and summer.

100 **Table 1.** Chemical reactions and rate constants used for the analysis of the chemical budgets of radicals.
 101 Values of reaction rate constants are given for standard conditions (298 K, 1 atm). Actual numbers are
 102 used for the calculations.

| | Reaction | $k(298\text{ K}, 1\text{ atm}) / \text{cm}^3\text{ s}^{-1}$ | $k_{\text{ERR}}^{\text{a}}$ | Reference |
|--|---|---|-----------------------------|-----------------------|
| Radical initiation reactions | | | | |
| R1 | $\text{HONO} + \text{h}\nu \rightarrow \text{OH} + \text{NO}$ | $j_{\text{HONO}}^{\text{b}}$ | | |
| R2 | $\text{O}_3 + \text{h}\nu \rightarrow \text{O}^1\text{D} + \text{O}_2$ | $j_{\text{O}^1\text{D}}^{\text{b}}$ | | |
| R2a | $\text{O}^1\text{D} + \text{H}_2\text{O} \rightarrow 2\text{OH}$ | 2.1×10^{-10} | $\pm 13\%$ | IUPAC |
| R2b | $\text{O}^1\text{D} + \text{M} \rightarrow \text{O}^3\text{P} + \text{M}$ | 3.3×10^{-11} | $\pm 10\%$ | IUPAC and JPL |
| R3 | $\text{HCHO} + \text{h}\nu \rightarrow 2\text{HO}_2 + \text{CO}$ | $j_{\text{HCHO}}^{\text{b}}$ | | |
| R4 | $\text{CH}_3\text{CHO} + \text{h}\nu \rightarrow \text{CH}_3\text{O}_2 + \text{HO}_2 + \text{CO}$ | $j_{\text{CH}_3\text{CHO}}^{\text{b}}$ | | |
| R5 | alkenes + $\text{O}_3 \rightarrow \text{OH}, \text{HO}_2, \text{RO}_2 + \text{products}$ | | | |
| R5a | propene + $\text{O}_3 \rightarrow \text{products}^{\text{c}}$ | 1.0×10^{-17} | $\pm 20\%$ | IUPAC |
| R5b | cis-but-2-ene + $\text{O}_3 \rightarrow \text{product}^{\text{d}}$ | 1.3×10^{-16} | $\pm 12\%$ | IUPAC |
| R5c | 1-pentene + $\text{O}_3 \rightarrow \text{products}^{\text{e}}$ | 1.0×10^{-17} | $\pm 20\%$ | MCMv3.3.1 |
| R5d | 2-hexene + $\text{O}_3 \rightarrow \text{products}^{\text{f}}$ | 1.1×10^{-17} | $\pm 20\%$ | MCMv3.3.1 |
| R5e | isoprene + $\text{O}_3 \rightarrow \text{products}^{\text{g}}$ | 1.3×10^{-17} | $\pm 10\%$ | MCMv3.3.1 |
| R5f | α -pinene + $\text{O}_3 \rightarrow \text{products}^{\text{h}}$ | 9.6×10^{-17} | $\pm 20\%$ | IUPAC |
| Radical interconversion reactions | | | | |
| R6 | $\text{HCHO} + \text{OH} + \text{O}_2 \rightarrow \text{CO} + \text{H}_2\text{O} + \text{HO}_2$ | 8.5×10^{-12} | $\pm 10\%$ | IUPAC |
| R7 | $\text{CO} + \text{OH} + \text{O}_2 \rightarrow \text{CO}_2 + \text{HO}_2$ | 2.3×10^{-13} | $\pm 6\%$ | IUPAC |
| R8 | $\text{VOCs} + \text{OH} + \text{O}_2 \rightarrow \text{RO}_2 + \text{H}_2\text{O}$ | j | | |
| R9 | $\text{RO}_2 + \text{NO} \rightarrow \text{products} + \text{HO}_2 + \text{NO}_2$ | 8.6×10^{-12} | $\pm 30\%$ | Jenkin et al. (2019) |
| R10 | $\text{HO}_2 + \text{NO} \rightarrow \text{OH} + \text{NO}_2$ | 8.5×10^{-12} | $\pm 13\%$ | IUPAC |
| R11 | $\text{HO}_2 + \text{O}_3 \rightarrow \text{OH} + 2\text{O}_2$ | 2.0×10^{-15} | $\pm 29\%$ | IUPAC |
| Radical termination reactions | | | | |
| R12 | $\text{NO}_2 + \text{OH} \rightarrow \text{HNO}_3$ | 1.0×10^{-11} | $\pm 30\%$ | IUPAC |
| R13 | $\text{NO} + \text{OH} \rightarrow \text{HONO}$ | 9.7×10^{-12} | $\pm 13\%$ | IUPAC |
| R14 | $\text{RO}_2 + \text{NO} \rightarrow \text{RONO}_2$ | 4.6×10^{-13} | $\pm 30\%$ | Jenkin et al. (2019) |
| R15 | $\text{RO}_2 + \text{RO}_2 \rightarrow \text{products}$ | 3.5×10^{-13} | $\pm 50\%$ | Jenkin et al. (2019) |
| R16 | $\text{RO}_2 + \text{HO}_2 \rightarrow \text{ROOH} + \text{O}_2$ | 2.3×10^{-11} | $\pm 50\%$ | Jenkin et al. (2019) |
| R17 | $\text{HO}_2 + \text{HO}_2 \rightarrow \text{H}_2\text{O}_2 + \text{O}_2$ | $4.5 \times 10^{-12\text{i}}$ | $\pm 20\%$ | IUPAC |
| Isoprene reactions | | | | |
| R18 | isoprene + $\text{OH} \rightarrow \text{products}$ | 1.0×10^{-10} | $\pm 8\%$ | IUPAC |
| R19 | isoprene- RO_2 (1,6-H shift) $\rightarrow \text{products}$ + OH | $0.01\text{--}0.06\text{ s}^{-1}$ | | Peeters et al. (2014) |
| Cl reactions | | | | |
| R20 | $\text{ClNO}_2 + \text{h}\nu \rightarrow \text{Cl} + \text{NO}_2$ | $j_{\text{ClNO}_2}^{\text{b}}$ | | |
| R21 | $\text{Cl}_2 + \text{h}\nu \rightarrow 2\text{Cl}$ | $j_{\text{Cl}_2}^{\text{b}}$ | | |
| R22 | $\text{VOCs} + \text{Cl} \rightarrow \text{RO}_2 + \text{HCl}$ | j | | |

103 ^a 1 σ uncertainty

104 ^b Measured photolysis frequencies

105 ^c Yield for OH: 0.36, HO₂: 0.10, RO₂: 0.42 from Novelli et al. (2021)

106 ^d Yield for OH: 0.36, HO₂: 0.15, RO₂: 0.51 from Novelli et al. (2021)

107 ^e Yield for OH: 0.32, HO₂: 0.09, RO₂: 0.37 from Novelli et al. (2021)

108 ^f Yield for OH: 0.48, HO₂: 0.11, RO₂: 0.59 from Novelli et al. (2021)

109 ^g Yield for OH: 0.26, HO₂: 0.26 from Malkin et al. (2010)

110 ^h Yield for OH: 0.8 from Cox et al. (2020)

111 ⁱ at 1% water vapour mixing ratio

112 ^j Highly variable depending on the specific VOC.

113

114 **2 Methodology**

115 **2.1 The JULIAC campaign**

116 The Jülich Atmospheric Chemistry Project (JULIAC) campaign was conducted at Forschungszentrum
 117 Jülich (FZJ, 50.9° N, 6.4° E), Germany. The project consisted of four one-month long intensive
 118 campaigns studying atmospheric chemistry in ambient air in each season throughout 2019. The location is
 119 surrounded by a deciduous forest and is located in a rural environment near a town, Jülich (33,000
 120 inhabitants), 25 km northeast, 40 km west, and 43 km southwest from three large cities, Aachen, Cologne
 121 and Düsseldorf, respectively. Therefore, ambient air is influenced by both biogenic and anthropogenic
 122 emission sources.

123 The investigation of the photochemistry was performed in the SAPHIR chamber, which was equipped
 124 with a large set of instruments measuring radicals, trace gases and aerosol (Table 2). The SAPHIR
 125 chamber has a cylindrical shape and is made of a double-wall Teflon (FEP) film. A slight overpressure
 126 (35 Pa) is maintained in the chamber and the space between the two films is permanently flushed with
 127 pure nitrogen (Linde, purity: > 99:99990 %) to prevent outside air penetrating the inner chamber. The

Table 2. Specification of instruments used in the JULIAC campaign for the analysis in this work.

| Species | Measurement technique | Time resolution(1 σ) | Limit of detection | 1 σ accuracy |
|--|--------------------------------|------------------------------|---|----------------------|
| OH | LIF | 270 s | $0.7 \times 10^6 \text{ cm}^{-3}$ | 18% |
| OH | DOAS | 134 s | $0.8 \times 10^6 \text{ cm}^{-3}$ | 6.5% |
| HO ₂ | LIF | 47 s | $1 \times 10^7 \text{ cm}^{-3}$ | 18% |
| RO ₂ | LIF | 47s | $2 \times 10^7 \text{ cm}^{-3}$ | 18% |
| OH reactivity (k_{OH}) | LP-LIF | 180 s | 0.2 s ⁻¹ | 10% |
| Photolysis frequencies | Spectroradiometer | 60 s | | 18% |
| O ₃ | UV photometry | 60 s | 0.5 ppbv | 2% |
| NO _x | Chemiluminescence ^a | 60 s | NO: 20 pptv | NO: 5 % |
| (NO+NO ₂) | | | NO ₂ : 30 pptv | NO ₂ : 7% |
| CO, CO ₂ , CH ₄ , H ₂ O | Cavity ring-down spectroscopy | 60 s | CO and CH ₄ : 1 ppbv CO ₂ : 25 ppbv H ₂ O: 0.1 % | 5% |
| HONO | LOPAP | 180 s | 5 pptv | 10% |
| HCHO | Cavity ring-down spectroscopy | 300 s | 0.1 ppbv | 10% |
| ClNO ₂ | I-CIMS | 60 s | 2.8 pptv | 8.5% |
| VOCs | PTR-TOF-MS | 30 s | 15 pptv | 14% |
| | VOCUS PTR-TOF-MS | 30 s | | |
| Aerosol surface area | SMPS | 7 min | 10nm – 1 μ m | N/A |

^a NO₂ was converted to NO before detection using a custom-built photolytic converter.

128 chamber is equipped with a shutter system allowing the air to be either shielded from or exposed to solar
129 radiation.

130 In the JULIAC campaign, ambient air was sampled at a high flow rate of $660 \text{ m}^3 \text{ h}^{-1}$ from 50 m high inlet
131 line (104 mm inner diameter, SilcoNert® coated stainless steel) by means of an oil-free turbo blower
132 (Aerzener Maschinenfabrik, AERZEN Turbo G3 Typ: TB 50-0.6 S). Large particles ($>10 \mu\text{m}$ diameter)
133 were removed by a SilcoNert® coated cyclone (LTG, ZSB-6). The temperatures in the inlet line and
134 cyclone were controlled to be slightly higher than ambient temperature (+1 to $2 \text{ }^\circ\text{C}$) to avoid water vapor
135 condensation in the inlet system. A 3/2-way valve directed part of the air (flow rate of $250 \text{ m}^3 \text{ h}^{-1}$) into the
136 chamber. Two fans inside the chamber ensured fast mixing on a time scale of a few minutes. As a result,
137 the chamber behaved as a continuously stirred photochemical flow reactor with a mean residence time of
138 air of 1.1 h. During the transition time of 3.5 s from the tip of the inlet to the SAPHIR chamber,
139 atmospheric RO_x radicals are lost on walls, but concentrations are rapidly re-established in the sampled
140 ambient air inside the sunlit chamber.

141 The use of the chamber as a flow reactor has advantages compared to field measurements in the open air.
142 Perturbations of the studied chemistry due to local emissions of VOCs or NO_x can be avoided. Transient
143 fluctuations of reactants in the sampled air, for example due to spikes of NO from passing cars, are
144 smoothed out in the chamber. Due to the homogeneous mixing, instruments connected to the chamber
145 measure the same air composition and segregation effects on reaction rates are insignificant.

146 The air composition could be influenced by the inlet line and chamber surfaces. As the whole inlet line is
147 heated and chemically inert due to the SilcoNert® coating, no relevant wall loss or desorption of trace
148 gases is expected from the inlet. This assumption was confirmed by comparing OH reactivity measured at
149 several positions of the inlet line. No significant differences were found between measurements, if the air
150 was either sampled upstream of the cyclone or downstream of the blower. Wall losses of trace gases
151 (VOCs, NO_x , O_3) inside the SAPHIR chamber were found to be negligible in previous experiments (e.g.,
152 Kaminski et al., 2017, Rolletter et al., 2020).

153 Nitrous acid (HONO) and formaldehyde (HCHO) are known to be emitted from the chamber film when it
154 is exposed to solar radiation (Rohrer et al. (2005)). These emissions significantly increase the
155 concentrations of HONO and HCHO in the chamber. Due to the transmission through the Teflon film and
156 shading from construction elements of the chamber, the absolute actinic flux density is reduced by 20 to
157 40 % compared to outside the chamber. It is worth noting, however, that the relative spectral distribution
158 of the solar radiation is not changed by the transmission through the chamber film (Bohn and Zilken,
159 2005).

160 The floor underneath the chamber is heated by the solar radiation. Although it is not in direct contact to
161 the foil, the air temperature in the chamber was on average 0.7°C higher during winter and autumn and
162 1.9°C higher during spring and summer than the temperature outside of the chamber at daytime. Since
163 photochemistry was studied in the chamber, all data of chemical and physical conditions shown in this
164 work refer to conditions inside the chamber.

165 The measurements in the campaign were at least once a week interrupted for calibration and maintenance
166 of instruments. Some days were also excluded from the analysis in this work because the chamber shutter

167 system was kept closed to protect the chamber film during bad weather from strong wind gusts and/or
168 precipitation. Reference experiments with clean synthetic air were performed to investigate possible
169 changes in the strength of chamber emissions and to check for instrumental backgrounds. In addition,
170 chemical actinometry experiments, in which NO₂ was photolyzed in synthetic air, were performed before
171 and after each intensive period. The comparison of actinometric and spectroradiometric j_{NO_2} values was
172 used to track and correct for changes in light transmission due to aging of the chamber wall (Bohn et al.,
173 2005).

174

175 **2.2 Instrumentation**

176 **2.2.1 OH, HO₂ and RO₂ radical and OH reactivity (k_{OH}) measurements**

177
178 OH, HO₂, and RO₂ radicals were measured by the FZJ – LIF which included a newly developed chemical
179 modulation reactor (CMR) for interference-corrected measurements of OH radicals (Cho et al., 2021).
180 The signals of the instrument were calibrated against well-defined radical concentrations that were
181 produced from water photolysis in synthetic air at a wavelength of 185nm using radiation of a mercury
182 lamp. A detailed description of the LIF instrument and its calibration can be found in previous
183 publications (Holland et al., 2003; Fuchs et al., 2008; Fuchs et al., 2011; Fuchs et al., 2012).

184 Shortly, the OH radical is sampled through a nozzle with a 0.4 mm diameter pinhole and is excited by a
185 pulsed laser at a wavelength of 308 nm in a low-pressure (4 hPa) fluorescence cell. The emitted resonant
186 fluorescence is detected with a time delay by a time-gated micro-channel plate detector (MCP). In the
187 JULIAC campaign, a chemical modulation reactor (CMR) was implemented on top of the OH cell to
188 quantify potential interferences. This is achieved by periodically removing ambient OH by an OH
189 scavenger that is injected in the reactor (propane, Air Liquide, purity>99.95%, (5.0±0.1) % mixture in
190 nitrogen) before the air enters the fluorescence cell. During the campaign, the observed interference could
191 be fully explained by the well-characterized interference from the photolysis of ozone in humid air inside
192 the detection cell. No evidence for an unexplained interference was found (Cho et al., 2021). The limit of
193 detection for OH was $0.7 \times 10^6 \text{ cm}^{-3}$ and the accuracy was 18 % (1σ).

194 OH radical concentrations were also measured by differential optical absorption spectroscopy (DOAS)
195 using a multiple folded light path for absorption inside along the chamber. The DOAS technique is a
196 calibration-free technique (Hausmann et al., 1997; Schlosser et al., 2007; Schlosser et al., 2009). The limit
197 of detection was $0.8 \times 10^6 \text{ cm}^{-3}$ and the 1σ -accuracy was 6.5 %. Due to a technical laser problem, the
198 DOAS instrument was not available in spring.

199 HO₂ radicals were detected by the LIF instrument in a separate detection cell, where HO₂ is chemically
200 converted to OH radicals in the reaction with NO (Air Liquide, 1% NO in N₂, purity > 99.5 %) that is
201 injected in the fluorescence cell (Fuchs et al., 2011). During the JULIAC campaign, two different
202 concentrations ($2.5 \times 10^{13} \text{ cm}^{-3}$ and $1.0 \times 10^{14} \text{ cm}^{-3}$) of NO in the fluorescence cell were used to
203 observe possible interference from specific RO₂ radicals as highlighted by Fuchs et al. (2011). No
204 difference between HO₂ measurements at high and low NO concentrations was found suggesting that
205 there was no significant interference from RO₂.

206 In addition, the sum of OH, HO₂, and RO₂ (RO_x) was measured by the RO_x-LIF system. Air is sampled
207 into a chemical converter (pressure of ~ 25 hPa), where a mixture of NO (Air Liquide, 500 ppmv NO in
208 N₂, purity > 99.5%) and CO (Air Liquide, 10% CO in N₂, purity > 99.997%) is injected. The NO converts
209 RO₂ radicals to HO₂ radicals and CO converts OH radicals formed from the reaction of HO₂ radicals with
210 NO back to HO₂. Therefore, an equilibrium between OH and HO₂ is established. Concentrations are
211 chosen, so that the equilibrium is on the side of HO₂. In a low-pressure cell downstream of the converter
212 HO₂ radicals are converted to OH radicals by injecting excess NO (Air Liquide, pure NO, purity>99.5%)
213 (Fuchs et al., 2008) that shifts the equilibrium between OH and HO₂ to OH. The RO₂ concentration is
214 obtained from the difference between the sum measurement of RO_x and measurements of OH and HO₂
215 concentrations in the other two detection cells. The RO₂ detection sensitivity was calibrated for methyl
216 peroxy radicals (CH₃O₂) which are produced from the reaction of OH with methane (CH₄) in the
217 calibration system. The resulting calibration is also applicable to the majority of other atmospheric alkyl
218 peroxy radicals (Fuchs et al., 2008; Fuchs et al., 2011) and recent laboratory tests performed with a
219 variety of VOCs including monoterpenes and chained alkanes for the CO and NO mixing ratios
220 applied in the RO_x converter during the JULIAC campaign showed a decrease of less than 15% of
221 sensitivity as compared to methyl peroxy radicals which is within the accuracy of the instrument.

222 The signals in the HO₂ and RO₂ detection systems contain a background signal observed when NO is
223 injected into the detection cells, even if no radicals are present in the air sampled. The background signal
224 can be characterized when the inlet of the detection system is overflowed with synthetic air, which is part
225 of the calibration procedures. During JULIAC the background varied from calibration to calibration and
226 was often larger than the smallest signals measured in ambient air from the chamber (Table S1). The
227 highest background signals obtained from calibrations is therefore regarded as an upper limit and the
228 variability is considered as an additional uncertainty in the measured HO₂ and RO₂ concentrations. HO₂
229 and RO₂ background signals, which are subtracted in the evaluation of HO₂ and RO₂ measurements, were
230 taken from reference experiments in the dark clean chamber, when no HO₂ or RO₂ radicals are expected.
231 The subtracted signals for each period are available in Table S1 and in most cases were equivalent to
232 concentrations lower than $1 \times 10^7 \text{ cm}^{-3}$ for both HO₂ and RO₂ measurements.

233 The total OH reactivity (k_{OH}), the inverse of the chemical lifetime of OH radicals, was measured in
234 ambient air by a laser-flash photolysis LIF instrument (Lou et al., 2010; Fuchs et al., 2017). A high
235 concentration of OH radicals is produced by flash photolysis (266 nm, 1 Hz repetition rate) of ozone in
236 humid air (Reaction R2) in a flow tube that is on top of an OH fluorescence cell. The pseudo first-order
237 decay of OH in the chemical reactions with atmospheric reactants is measured, giving directly the OH
238 reactivity.

239 **2.2.2 Other trace gases, aerosol properties and photolysis frequencies measurements**

240 A comprehensive set of instruments operated during the JULIAC campaign (Table 2) analyzed the air
241 composition inside the chamber. Photolysis frequencies inside the chamber were derived from solar
242 actinic flux densities measured by a spectroradiometer mounted on the roof of the nearby institute
243 building. Chamber values were calculated using a model approach considering shading effects and the
244 influence of the chamber film (Bohn et al., 2005; Bohn and Zilken, 2005). Formaldehyde (HCHO) was
245 detected by cavity ring-down spectroscopy (Picarro, G2307, Glowania et al. (2021)). NO and NO₂ were
246 measured by chemiluminescence (Eco Physics, TR780, NO₂ conversion by a custom-built photolytic

247 converter). In addition, HONO was measured by long-path absorption photometry (LOPAP, Kleffmann et
 248 al. (2006); Häsel et al. (2009)), CO, CO₂, CH₄, and H₂O by cavity ring-down spectroscopy (Picarro,
 249 G2401), and O₃ by UV absorption (Ansyco-41M and Thermo scientific-49I). Volatile organic compounds
 250 (VOCs) were detected by a proton-transfer-reaction time-of-flight mass spectrometer (PTR-TOF-MS,
 251 Ionicon) (Jordan et al., 2009) and a VOCUS PTR-TOF-MS instrument (Aerodyne). The VOCs included
 252 in this study are listed in Table S2 and include isoprene and some carbonyl compounds. Total aerosol
 253 surface area was determined from measurements by a scanning mobility particle sizer (SMPS). In the
 254 summer and autumn periods, nitryl chloride (ClNO₂) was detected by a chemical ionization mass
 255 spectrometer using iodine as reagent ion (I-CIMS) (Sommariva et al., 2018; Tan et al., 2022).

256 In addition to measurements in the chamber, concentrations of O₃ and NO_x were also measured in the
 257 inlet system before the air flowed into the SAPHIR chamber. For these measurements, a combined system
 258 (Eco Physics, CraNO_x) consisting of an ozone photometer and a chemiluminescence instrument for NO_x
 259 was deployed. Measurements were used to determine the photochemical ozone production in the JULIAC
 260 campaign. Further description of the measurement set-up and concept of the evaluation will be discussed
 261 in details in a further publication.

262

263 2.3 Chemical budget calculations

264 A chemical budget analysis, similar as in Tan et al. (2019) and Whalley et al. (2021), was applied for OH,
 265 HO₂, RO₂ and the sum of all three radicals (RO_x) to the data set from the JULIAC campaign. All
 266 reactions typically considered to be relevant for the generation and destruction of these radicals are
 267 considered (Table 1). Rate constants and their uncertainties were mainly taken from IUPAC
 268 recommendations (Atkinson et al., 2004; Atkinson et al., 2006; Cox et al., 2020) or more recent studies. If
 269 not otherwise specified, radical production and destruction rates are calculated from measured
 270 concentrations of reactants.

271 2.3.1 Chemical budget of OH radicals

272 The production rate of OH radicals includes primary production reactions (Reaction R1, R2 and R5) and
 273 radical interconversion reactions (Reaction R10 and R11):

$$274 P_{\text{OH}} = j_{\text{HONO}}[\text{HONO}] + \varphi_{\text{OH}} j_{\text{O}^1\text{D}}[\text{O}_3] + k_{10}[\text{NO}][\text{HO}_2] + k_{11}[\text{O}_3][\text{HO}_2] \\
 275 + \Sigma\{\varphi_{\text{OH}}^i k_5^i [\text{alkene}]^i [\text{O}_3]\} + P_{\text{OH,Isop.}} \quad (1)$$

276 Here, φ_{OH} is the effective OH yield of the ozone photolysis including the reaction of excited oxygen
 277 atoms O(¹D) with H₂O producing two OH radicals. φ_{OH}^i is the OH yield of the ozonolysis reaction of
 278 alkenes, and k_5^i represents the rate constants of the corresponding reactions.

279 $P_{\text{OH,Isop}}$ is the effective production of OH radicals from unimolecular reactions (1,6-hydrogen shift
 280 reactions) of isoprene-RO₂ radicals (Z- δ -RO₂-I and II, Peeters et al. (2014)) and the subsequent chemistry
 281 of products.. As there was no measurement of speciated RO₂ radicals, isoprene-RO₂ radical
 282 concentrations are estimated from steady-state conditions considering their production from the reaction

283 of isoprene with OH and their destruction in bimolecular reaction (reaction rate k_{bi}) and unimolecular
 284 reactions (bulk reaction rate $k_{bulk\ 1,6-H}$ as defined in Peeters et al. (2014)):

$$285 \quad [RO_2(isop.)]_{SS} = \frac{k_{18}[Isoprene][OH]}{k_{bi} + k_{bulk\ 1,6-H}} \quad (2)$$

$$286 \quad k_{bi} = (k_9 + k_{14})[NO] + k_{15}[RO_2] + k_{16}[HO_2] \quad (2a)$$

287 Bimolecular loss reactions include reactions with NO (Reaction R9 and R14), RO₂ (Reaction R15) and
 288 HO₂ (Reaction R16). The OH production from isoprene-RO₂ isomerization reactions is simplified in the
 289 calculation of the total OH production in this work by assuming that each isomerization reaction produces
 290 rapidly one OH radical from the subsequent reactions of products such as photolysis of hydroxy-peroxy
 291 aldehyde (HPALD). In this case, the radical production rate is equal to the loss rate of the isoprene-RO₂
 292 due to isomerization reactions ($D_{Z-\delta-RO_2,Isop.}$):

$$293 \quad P_{OH,Isop.} = D_{Z-\delta-RO_2, Isop.} = k_{bulk\ 1,6-H} [RO_2(isop.)]_{SS} \quad (4)$$

294 The total loss rate of OH radicals for the chemical budget analysis is determined by the product of the
 295 total OH reactivity (k_{OH}) and the OH radical concentration:

$$296 \quad D_{OH} = k_{OH}[OH] \quad (5)$$

297 **2.3.2 Chemical budget of HO₂ radicals**

298 The production rate of HO₂ radicals includes primary reactions (Reaction R3, R4 and R5) and
 299 interconversion reactions (Reaction R6, R7 and R9, Table 1):

$$301 \quad P_{HO_2} = 2 j_{HCHO}[HCHO] + k_6[HCHO][OH] + k_7[CO][OH] + k_9[NO][RO_2] \\ 300 \quad \quad \quad + \sum\{\varphi_{HO_2}^i k_5^i [alkene]^i [O_3]\} \quad (6)$$

302 Here, the photolysis frequency of HCHO (j_{HCHO}) include only paths generating radicals. $\varphi_{HO_2}^i$ is the
 303 HO₂ yield from the ozonolysis of alkenes. The reactions of OH with H₂ and O₃ are not considered due to
 304 their negligible contributions to the HO₂ production.

305 The loss rate of HO₂ is determined by the reactions with NO (Reaction R10), O₃ (Reaction R11), RO₂
 306 (Reaction R16) and HO₂ (Reaction R17):

$$307 \quad D_{HO_2} = (k_{10}[NO] + k_{11}[O_3] + k_{16}[RO_2] + 2k_{17}[HO_2])[HO_2] \quad (7)$$

308 Here, the humidity dependence of k_{17} was taken into account. The reaction of HO₂ radicals with NO₂ is
 309 not included as the thermal decomposition of peroxyxynitric acid (HO₂NO₂) forming back HO₂ radicals and
 310 NO₂ is instantaneous for the temperatures experienced during the JULIAC campaign.

311 In a sensitivity calculation (Section 4.2.3), potential loss of HO₂ due to heterogeneous uptake on aerosol
 312 is investigated. The first order loss rate ($k_{het.}$) can be described as:

$$313 \quad k_{het.} = \frac{Y_{eff.} \cdot \nu_{HO_2} \cdot [AS]}{4} \quad (8)$$

314 v_{HO_2} is the mean molecular velocity of HO_2 ($4.44 \times 10^5 \text{ cm s}^{-1}$ at 298 K), $[\text{AS}]$ is the measured aerosol
315 surface area concentration, and γ_{eff} is the effective uptake coefficient.

316 2.3.3 Chemical budget of RO_2 radicals

317 Primary sources of RO_2 radicals include all oxidation reactions of VOCs with OH, Cl, NO_3 radicals and
318 O_3 . As the number of measured VOC species in this study was limited (Table S2) and because it is
319 generally difficult to capture the entire spectrum of atmospheric VOCs (Goldstein and Galbally, 2007;
320 Lou et al., 2010), the measured total OH reactivity (k_{OH}) can be used to calculate the RO_2 radicals
321 production from the reactions of VOCs with OH. First, the contributions from CO, NO, NO_2 , HCHO and
322 O_3 is removed from the measured OH reactivity as these species do not form RO_2 radicals in the reaction
323 with OH. It is then assumed that the remaining fraction can be attributed to organic compounds (VOC
324 reactivity (k_{VOC})) including measured and unmeasured VOCs, which produce RO_2 radicals in their
325 reaction with OH.

326 For some aromatics, such as toluene, benzene, xylene, etc., the prompt formation of HO_2 is expected by
327 their reaction with OH (Nehr et al., 2011; Nehr et al., 2014; Jenkin et al., 2019). However, in this
328 campaign, their concentrations were small and their average contributions to the OH reactivity from
329 VOCs were only 2.8%. Therefore, their potential impacts on the RO_2 production are negligible (less than
330 1%).

331 In addition, RO_2 production from ozonolysis needs to be included. In this work, only the reactions of
332 measured organic compounds are considered. The contribution to the RO_2 production from the oxidation
333 of VOCs by the NO_3 radical was negligible during daytime due to the low VOC load (low OH reactivity),
334 so that NO_3 destruction by photolysis and reaction with NO dominated.

335 Reactions of chloride (Cl) also produce RO_2 radicals, but the concentration was not measured in the
336 JULIAC campaign. However, one of the most important precursor species, nitryl chloride (ClNO_2), was
337 detected during the campaign (except in spring, Tan et al. (2022)). ClNO_2 can accumulate during
338 nighttime, but it is photolyzed after sunrise yielding NO_2 and Cl atoms (Reaction R20). Assuming as an
339 upper limit that each Cl atom reacts with a VOCs (Tanaka et al., 2003), the RO_2 production rate from Cl
340 radicals can be calculated as:

$$341 P_{\text{RO}_2, \text{Cl}} = j_{\text{ClNO}_2} [\text{ClNO}_2] \quad (9)$$

342 The total RO_2 production rate is then calculated as:

$$343 P_{\text{RO}_2} = k_{\text{VOC}} [\text{OH}] + \sum (\varphi_{\text{RO}_2}^i k_{\text{R5}}^i [\text{alkene}]^i [\text{O}_3]) + P_{\text{RO}_2, \text{Cl}} \quad (10)$$

344 Here, $\varphi_{\text{RO}_2}^i$ is the RO_2 yield from the ozonolysis of alkenes species (Table 1).

345 With respect to the destruction rate of RO_2 , its reactions with NO, HO_2 , and other RO_2 and unimolecular
346 reactions of specific isoprene- RO_2 radicals ($D_{\text{Z}-\delta-\text{RO}_2, \text{Isop}}$) (Eq. 4) are considered in this work:

$$347 D_{\text{RO}_2} = ((k_9 + k_{14}) [\text{NO}] + 2k_{15} [\text{RO}_2] + k_{16} [\text{HO}_2]) [\text{RO}_2] + D_{\text{Z}-\delta-\text{RO}_2, \text{Isop}} \quad (11)$$

348 2.3.4 Chemical budget of RO_x radicals

349 In the chemical budget of the sum of OH, HO₂ and RO₂ (RO_x), inter-radical conversion reactions cancel
350 out and only initiation and termination reactions are included. Therefore, the RO_x radical budget analysis
351 allows to investigate if primary radical source reactions or termination processes are missing in the
352 chemical mechanism used (Table 1).

353 The production rate of the RO_x radicals is given by the sum of rates from radical initiation reactions
354 (Reaction R1-R5, R20-R22, Table 1):

$$355 P_{RO_x} = j_{HONO}[HONO] + \varphi_{OH}j_{O^1D}[O_3] + 2j_{HCHO}[HCHO] \\ 356 + \sum((\varphi_{OH}^i + \varphi_{HO_2}^i + \varphi_{RO_2}^i)k_5^i[\text{alkene}]^i[O_3]) + P_{RO_2,Cl} \quad (12)$$

357 Radicals can be additionally produced from the photolysis of other oxygenated organic compounds
358 (OVOCs, e.g., Reaction R4) not included in Eq. 12. Their potential impact is further discussed in Section
359 4.2.2.

360 The loss rate of the RO_x radical is calculated by the sum of rates from radical termination reactions
361 (Reaction R12-R17):

$$362 D_{RO_x} = (k_{13}[NO] + k_{12}[NO_2])[OH] + k_{14}[NO][RO_2] + 2k_{15}[RO_2]^2 + 2k_{16}[HO_2][RO_2] + 2k_{17}[HO_2]^2 \\ 363 \quad (13)$$

364 **2.3.5 Uncertainties in the calculated production and destruction rates**

365 The uncertainty of each production or loss rate is calculated by Gaussian summation of the 1σ errors of
366 the measured quantities (Table 2) and the uncertainties of the reaction rate constants (Table 1).

367 For reactions of RO₂ with NO (Reaction R9, R14), HO₂ (Reaction R16) and RO₂ (Reaction R15), generic
368 rate constants are used for the sum of RO₂ radicals (Table 1, Jenkin et al. (2019)). Rate constants of the
369 NO reaction with RO₂ derived from hydrocarbons (<C₅) and with oxygenated peroxy radicals range from
370 $7.7 \times 10^{-12} \text{ cm}^3 \text{ s}^{-1}$ to $1.1 \times 10^{-11} \text{ cm}^3 \text{ s}^{-1}$ (Jenkin et al., 2019). The 1σ-uncertainty of the rate constants
371 varies from 6 to 30 %. In the error calculations here, an upper limit value of 30 % is applied. However,
372 for reactions of RO₂ with HO₂ and with RO₂, the range of rate constants varies by more than an order of
373 magnitude. In the calculations, an uncertainty of 50% is used for the reaction rate constants of RO₂ with
374 HO₂ and with RO₂.

375 As there are no measurements of speciated RO₂ radicals, a yield of 5% for the formation of organic
376 nitrates is assumed for all RO₂ but the yield can vary between 1% for methyl peroxy radicals (CH₃O₂) and
377 more than 20 % for RO₂ from monoterpene species. This simplification can introduce systematic errors in
378 the calculations (Section 4.2.1).

379

380 **2.4 Odd oxygen production rate**

381 In the troposphere, ozone is formed exclusively by the oxidation of NO to NO₂ through reaction with RO₂
382 (Reaction R9) and HO₂ (Reaction R10), followed by NO₂ photolysis (Fishman and Carney, 1984; Sillman
383 et al., 1990; Kleinman et al., 2002).

384 During the day, the photolysis of NO₂ and the back reaction of NO with O₃ form a rapid photochemical
385 equilibrium between O₃ and NO₂. The sum of O₃ and NO₂ is therefore defined as odd oxygen (O_X) (Han
386 et al., 2011; Goldberg et al., 2015). The relative composition of O_X depends on the NO₂ photolysis
387 frequency and the NO concentration. For the conditions of the spring and summer periods in the JULIAC
388 campaign, O_X consisted predominantly (> 85%) of O₃.

389 In this work, the net production rate of O_X (P_{O_X}) was determined experimentally from the increase of O_X
390 in the sunlit SAPHIR chamber. Furthermore, measurements of radicals and NO_X were used to calculate
391 P_{O_X} from the rate of O_X formation reactions (Reaction R9, R10), and O_X loss by the reaction of NO₂ with
392 OH (Reaction R12) (Mihelcic et al., 2003; Cazorla et al., 2012; Niether et al., 2022)):

$$393 \quad P_{O_X,net} = k_9[NO][RO_2] + k_{10}[NO][HO_2] - k_{12}[NO_2][OH] \quad (14)$$

394 This calculation neglects minor O_X destruction processes such as the reaction of O₃ with NO₂, OH, HO₂,
395 Cl or alkenes since they did not play a notable role during the day in this campaign.

396 **3 Results**

397 **3.1 Data quality of radical measurements**

398 Performing measurements in the SAPHIR chamber allowed to test the accuracy of radical measurements
399 in different ways that are typically not available in field experiments. First, OH radicals was measured by
400 2 independent instruments, the OH-DOAS and LIF instruments (Cho et al., 2021). Second, the O_X
401 production rate calculated from measured concentrations of HO₂ and RO₂ could be compared to the
402 observed increase of O_X concentrations in the chamber, which can be solely attributed to chemical
403 reactions. This is possible, because other factors typically impacting the O_X concentration in field
404 experiments such as transportation processes are not effective.

405 OH concentrations were measured by the LIF instrument applying the chemical modulation scheme and
406 the DOAS in the winter, summer and autumn periods of the campaign. As OH concentrations were close
407 to the limit of detection in autumn and winter, a meaningful comparison of measurements was only
408 possible for the summer period. A detailed comparison of measurements can be found in Cho et al. (2021).
409 In general, the OH measurements of the two instruments agreed within their measurement errors (Table 1)
410 giving a slope of 1.1±0.02 in a linear regression analysis. The good agreement confirms that the newly
411 developed chemical modulation system of the LIF instrument allowed for interference-free OH
412 concentration measurements for conditions of the campaign. Only in the period from 22 to 26 August,
413 which was characterized by exceptionally high temperatures (30 to 40°C), OH concentrations measured
414 by the LIF instrument were systematically higher by 25% than those measured by the DOAS instrument
415 for unknown reasons (Cho et al., 2021). OH concentrations measured by the DOAS instrument were used
416 for the analysis of the radical budgets in this period.

417 Net O_X production rates were determined from the measured increase of O_X concentrations in the
418 chamber and compared to calculations from the turnover rates of HO₂ and RO₂ reactions with NO. This
419 calculation takes also the NO₂ loss due to its reaction with OH into account (Eq. 14). The odd oxygen
420 production rate did not exceed 1 ppbv h⁻¹ in winter and autumn due to the general low photochemical

421 activity in these seasons. In spring and summer, the O_x production rate showed clear diurnal variations
 422 with noontime maxima that reached up to 16 ppbv h^{-1} . In these seasons, both methods for determining the
 423 O_x production rate agreed within $\pm 15 \%$ (1σ). Observed discrepancies were less than 1 ppbv h^{-1} , when
 424 NO mixing ratios were lower than 1 ppbv , but reached values of 3 ppbv h^{-1} for NO mixing ratios of $3 - 4$
 425 ppbv NO . The largest discrepancy of 8.5 ppbv h^{-1} was found in the morning on 29 April, when the NO
 426 mixing ratio exceeded 9 ppbv . High NO values suppressed HO_2 and RO_2 concentrations to values below
 427 $2.0 \times 10^7 \text{ cm}^{-3}$, which is within the range of the background corrections for the HO_2 and RO_2
 428 measurements (Table S1). Under these conditions, an erroneous background subtraction may have caused
 429 the observed discrepancies.

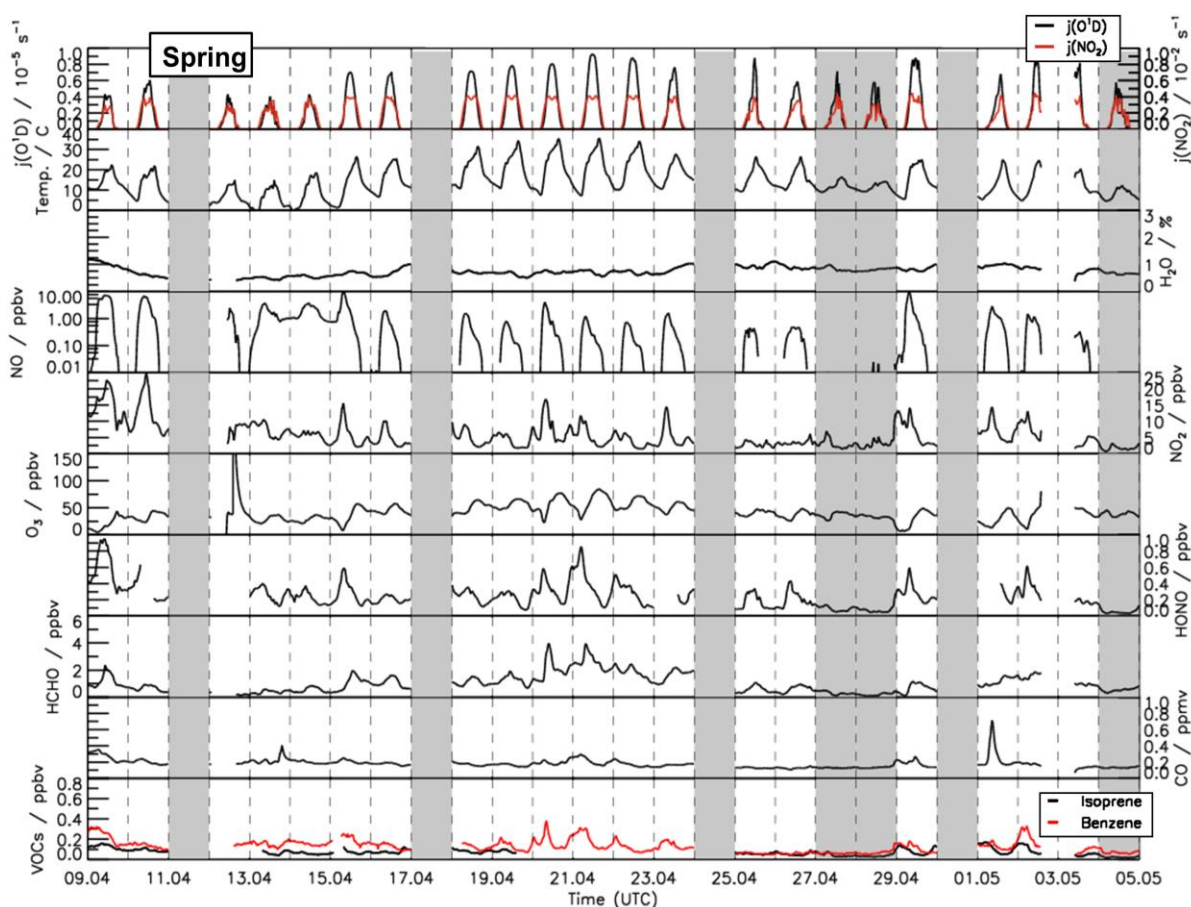


Figure 1: Time series of temperature and trace gas concentrations during the spring period of the JULIAC campaign (Cho et al., 2022). Vertical dashed lines denote midnight. Grey shaded areas indicate calibration days, when no measurements were done and days when the chamber roof was closed due to bad weather conditions.

430

431 3.2 Meteorological and chemical conditions during the JULIAC campaign

432 A broad range of meteorological and chemical conditions was encountered during the JULIAC campaign.
 433 During the winter and autumn periods (Fig. S1 and S2), the sky was often overcast and it rained

434 frequently. Temperatures were generally below 10°C and the photolysis frequencies of ozone (j_{O_3}) and
435 nitrogen dioxide (j_{NO_2}) mostly remained below $1.5 \times 10^{-6} \text{ s}^{-1}$ and $2 \times 10^{-3} \text{ s}^{-1}$, respectively. During
436 spring and summer, temperatures in the chamber were up to 35°C in mid-April and 40°C between 24 and
437 31 August (Fig. 1 and 2). Photolysis frequencies in the chamber were $1 \times 10^{-5} \text{ s}^{-1}$ (j_{O_3}) and $4 \times 10^{-3} \text{ s}^{-1}$
438 (j_{NO_2}).

439 The air was sampled at all times from 50 m above ground. The temperature at different heights measured
440 between 5 m and 120 m at a meteorological tower near the SAPHIR chamber showed that the air was
441 well mixed within this height range during the day. Therefore, it can be assumed for the chemical
442 composition of the air sampled into the chamber to be representative for the air within the atmospheric
443 boundary layer. At night, vertical temperature profiles showed atmospheric stratification below 100 m.
444 The air at 50 m can be assumed to be isolated from the ground and therefore not being affected by surface
445 emissions or deposition on surfaces at the ground.

446 Overall, relatively clean air was sampled during the whole JULIAC campaign indicated by CO and NO
447 mixing ratios below 0.3 ppmv and 2 ppbv, respectively. Concentrations of anthropogenic organic
448 compounds (e.g. benzene and toluene) were low with mixing ratios of less than 0.5 ppbv. Even though the
449 measurement site is surrounded by a deciduous forest, the concentrations of biogenic organic compounds
450 such as isoprene and monoterpenes were also low (median 0.8 ppbv and 0.15 ppbv, respectively)
451 compared to previously reported values measured on the campus of FZJ in summer, when isoprene
452 concentrations ranged between 0.5 to 4 ppbv (Komenda et al., 2003; Spirig et al., 2005; Kanaya et al.,
453 2012). A possible reason for the low values could be damages of trees from severe droughts in the
454 previous year (BMEL, 2021).

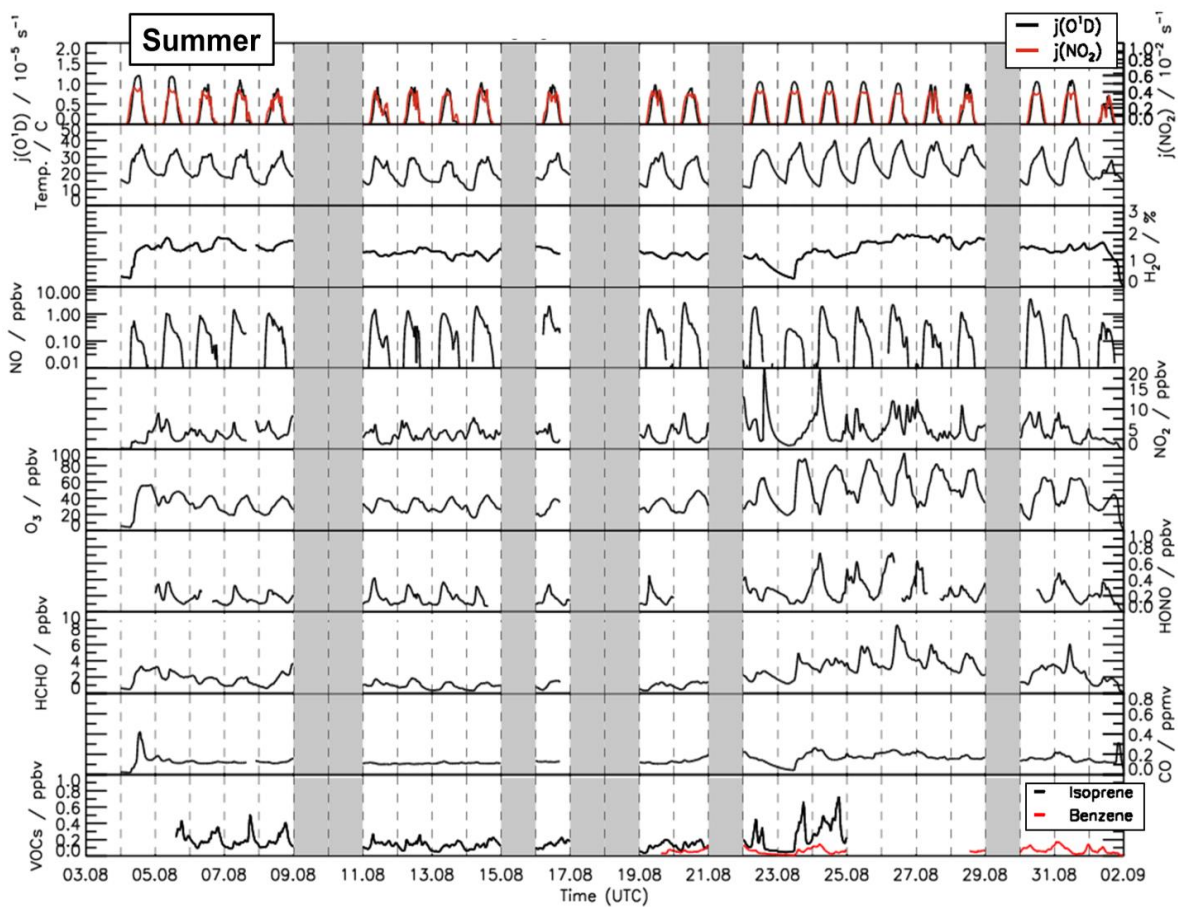


Figure 2: Time series of temperature and trace gas concentrations during the summer period of the JULIAC campaign (Cho et al., 2022). Vertical dashed lines denote midnight. Grey shaded areas indicate calibration days, when no measurements were done and days when the chamber roof was closed due to bad weather conditions.

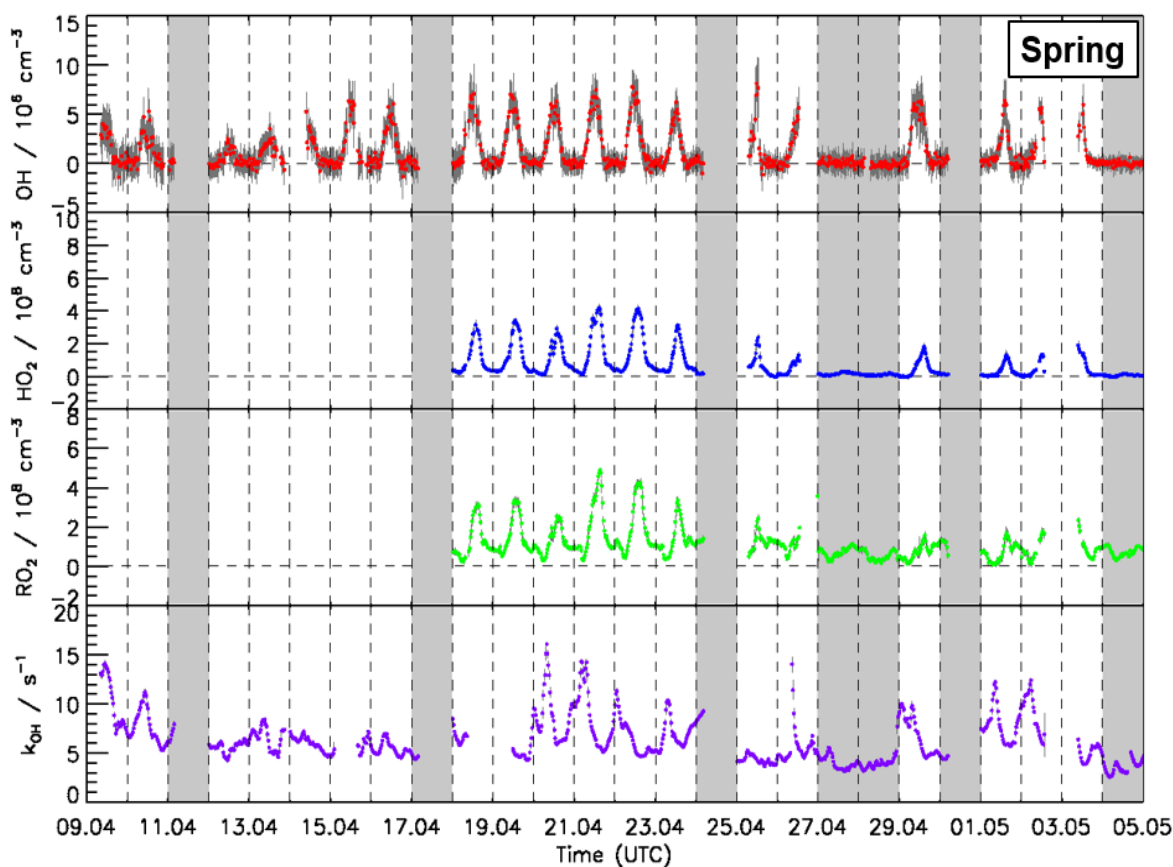


Figure 3: Time series of OH, HO₂, and RO₂ radical concentration measured by the FZJ-LIF-CMR instrument and measurements of the OH reactivity (k_{OH}) measured in the spring period of the JULIAC campaign (Cho et al., 2022). Vertical bars represent 1σ statistical errors. Vertical dashed lines denote midnight. Grey shaded areas indicate calibration days when no measurements were done and days when the chamber roof was closed due to bad weather conditions.

456 3.3 OH, HO₂, and RO₂ radical concentrations and OH reactivity during winter and autumn periods 457 of the JULIAC campaign

458 During winter (Fig. S3) and autumn (Fig. S4), daytime OH radical concentrations were below $1 \times$
 459 10^6 cm^{-3} , mainly due to a low primary radical production. Daytime peroxy radical (HO₂ and RO₂)
 460 concentrations during these periods were also very low with average values below $2 \times 10^7 \text{ cm}^{-3}$ (Fig. S5)
 461 close to the limit of detection of RO₂ radicals (Table 2) and within the uncertainty of the background
 462 corrections for HO₂ and RO₂ (Table S1). During winter and autumn, HO₂ concentrations typically
 463 increased in the morning and reached peak concentrations of $2 \times 10^7 \text{ cm}^{-3}$ at noon. Concentrations
 464 decreased in the evening and night with minimum values right before sunrise. In contrast, nighttime RO₂
 465 concentrations increased to values between 3 to $4 \times 10^7 \text{ cm}^{-3}$ after sunset, when the chemical loss due to
 466 their reaction with NO became negligible, while RO₂ radicals were still produced from reactions of VOC
 467 with NO₃ and O₃. NO concentrations were essentially zero at that time, because NO production by the
 468 photolysis of NO₂ stopped and NO rapidly reacted with ozone. RO₂ radical concentrations decreased in

469 the morning to values that were similar to that of HO₂ radicals as can be expected for conditions with high
470 NO mixing ratios, which lead to a fast loss of RO₂ and HO₂ in their reactions with NO.

471 The measured OH reactivity (k_{OH}) ranged between 4 and 33 s⁻¹ during winter and autumn periods. The
472 highest value was observed on 21 January, when a highly polluted plume containing 50 ppbv of NO was
473 sampled.

474 The measured OH reactivity can be compared to OH reactivity calculated by summing up the product
475 between measured OH reactant concentrations and their reaction rate constants with the OH radical. On
476 average, 1.3 s⁻¹ (18 %) of the measured OH reactivity could not be explained by the measured OH
477 reactants during the winter and autumn periods (Fig. S5). NO_x, CH₄, CO, and VOCs contributed
478 approximately 43, 3, 20 and 13 %, respectively, to the measured OH reactivity.

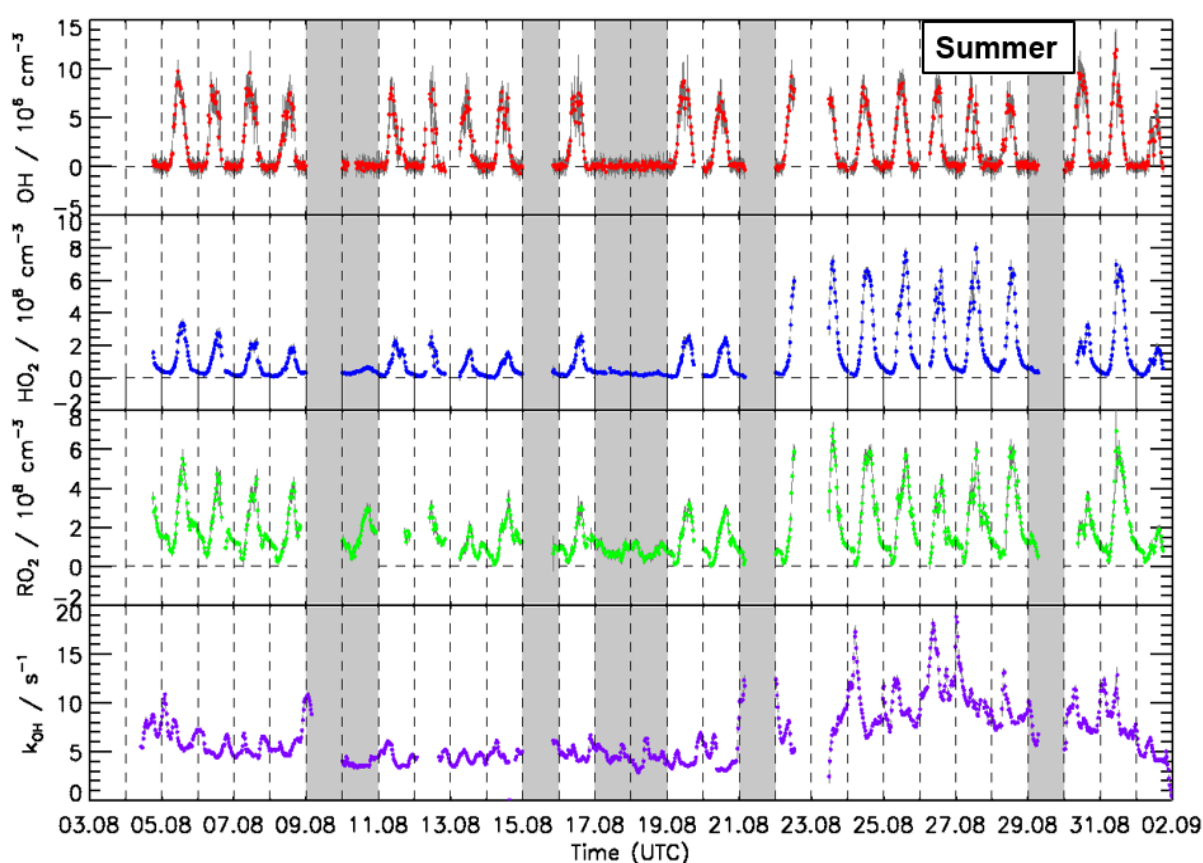


Figure 4: Time series of OH, HO₂, and RO₂ concentration measured by the FZJ-LIF-CMR instrument and measurements of the OH reactivity (k_{OH}) in the summer period of the JULIAC campaign (Cho et al., 2022). Vertical bars represent 1 σ statistical errors. Vertical dashed lines denote midnight. Grey shaded areas indicate calibration days when no measurements were done and days when the chamber roof was closed due to bad weather conditions.

479

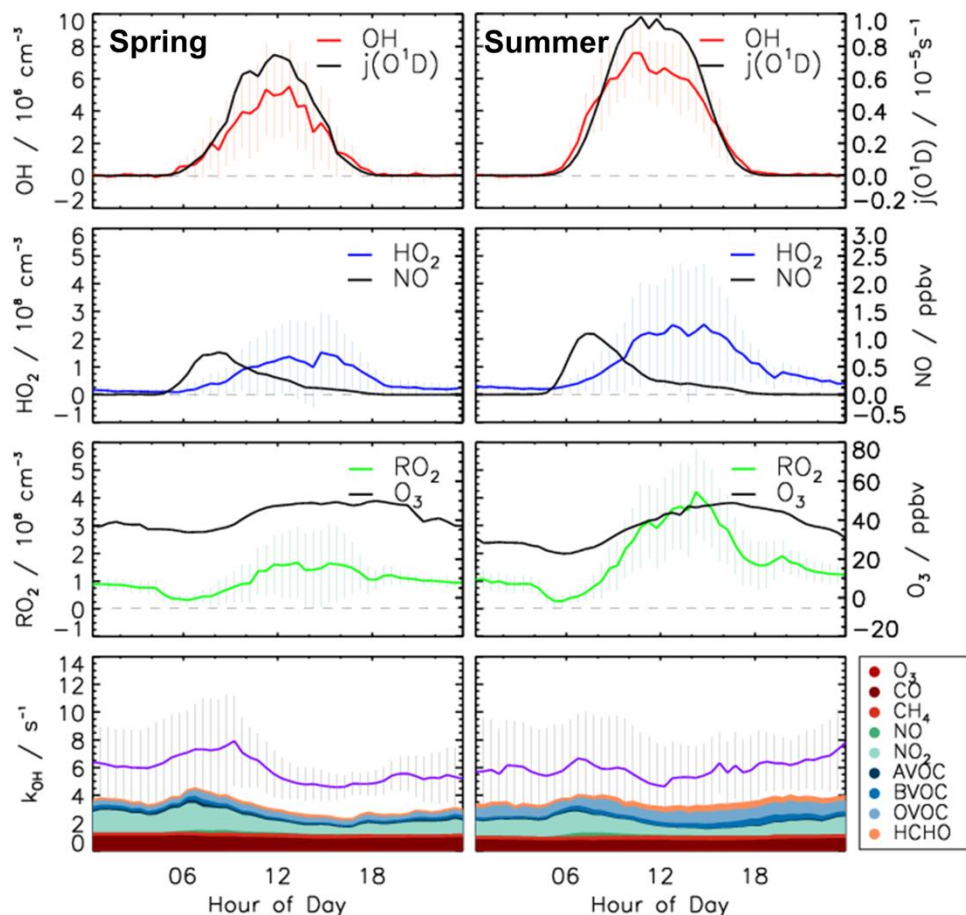


Figure 5: Median values of the diurnal profiles of OH, HO₂, RO₂, k_{OH}, j_{OH}, NO and O₃ measured in the spring and summer periods of the JULIAC campaign. Colored areas represent the contributions of measured reactants to the total OH reactivity. Vertical lines give 25th and 75th percentile values.

480

481 3.4 OH, HO₂, and RO₂ radical concentrations and OH reactivity during the spring and summer 482 periods of the JULIAC campaign

483 During spring and summer (Fig. 3, 4 and 5), maximum daytime OH concentrations were between 6 and 8
484 $\times 10^6 \text{ cm}^{-3}$. The highest OH concentration ($1.2 \times 10^7 \text{ cm}^{-3}$) occurred on 31 August. The diurnal OH
485 concentration profile shows a high correlation with the ozone photolysis frequency (j_{O^1D}) as observed in
486 previous field campaigns (e.g., Ehhalt and Rohrer (2000); Handisides et al. (2003); Holland et al. (2003)).

487 Unfortunately, the measurements of HO₂ and RO₂ radicals were not available for the first two weeks of
488 the spring campaign due to a malfunction of the instrument. Daily maximum HO₂ and RO₂ concentrations
489 were in the range of 2 to 4 $\times 10^8 \text{ cm}^{-3}$ during the spring period and the first half of the summer period.
490 Maximum HO₂ and RO₂ concentrations were $8.0 \times 10^8 \text{ cm}^{-3}$ and $7.0 \times 10^8 \text{ cm}^{-3}$, respectively, during
491 the second half of summer period. In spring and summer, peroxy radical concentrations showed a distinct
492 diurnal pattern. Both HO₂ and RO₂ radical concentrations were suppressed in the early morning (between
493 04:00 and 07:00) due to the reaction with elevated NO mixing ratios of up to 1.5 ppbv. Maximum peroxy

494 radical concentrations were usually reached in the afternoon (~14:00), when NO concentrations were
495 lowest.

496 The measured OH reactivity values were in the range of 4 to 18 s⁻¹. High values were observed between
497 23 and 31 August due to high emissions of biogenic volatile organic compounds (BVOCs) from plants at
498 high ambient temperatures. The OH reactivity that cannot be attributed to the measured OH reactants was
499 on average, 2.5 s⁻¹ (40%), which is much higher than observed in the winter and autumn periods (Fig. S5).
500 CO and CH₄ contributed 10% and 4%, respectively. Due to the high emissions of biogenic organic
501 compounds in spring and summer, the attributed contribution of organic compounds to the total measured
502 OH reactivity was 20 % and the contribution of NO_x was only 19 %, much less compared to the winter
503 and autumn periods. Isoprene had the largest contribution among all VOCs accounting for up to 5 % of
504 the total measured OH reactivity. Unfortunately, the number of detected VOC species in the JULIAC
505 campaign was small (Table S2).

506 In the JULIAC campaign, nighttime OH concentrations were clearly below the limit of detection of the

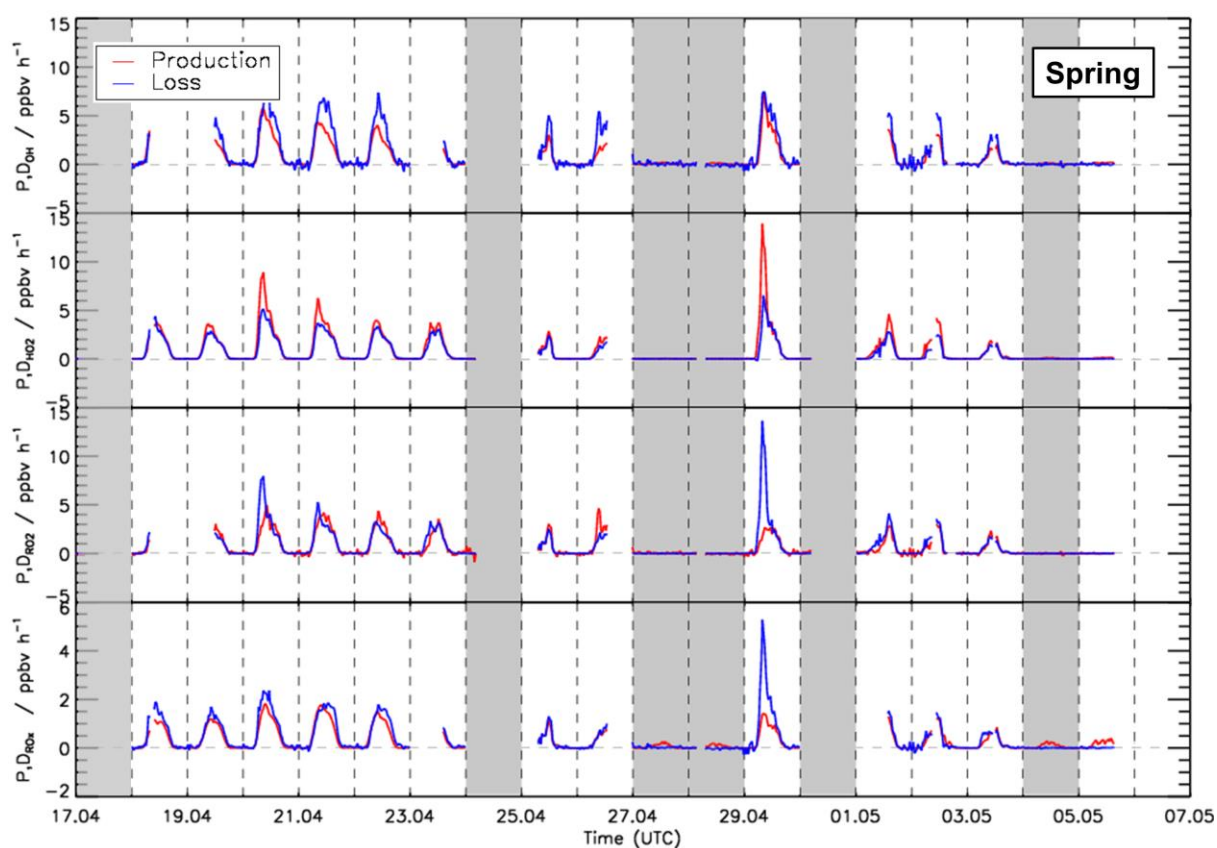


Figure 6: Time series of total production and destruction rates of OH, HO₂, RO₂, and RO_x radicals in the spring period of the JULIAC campaign. Vertical dashed lines denote midnight. Grey areas indicate calibration days and days when the chamber roof was closed.

507 FZJ-CMR-LIF instrument ($0.7 \times 10^6 \text{ cm}^{-3}$). When all nighttime data are averaged, mean OH
508 concentrations with 1σ standard errors of $(3 \pm 1) \times 10^4 \text{ cm}^{-3}$ and $(5 \pm 3) \times 10^4 \text{ cm}^{-3}$ are obtained for
509 the spring and summer periods, respectively. These low values support the absence of instrumentally

510 produced OH and indicate a very low nocturnal OH production at 50 m height in the absence of NO and
 511 solar UV.

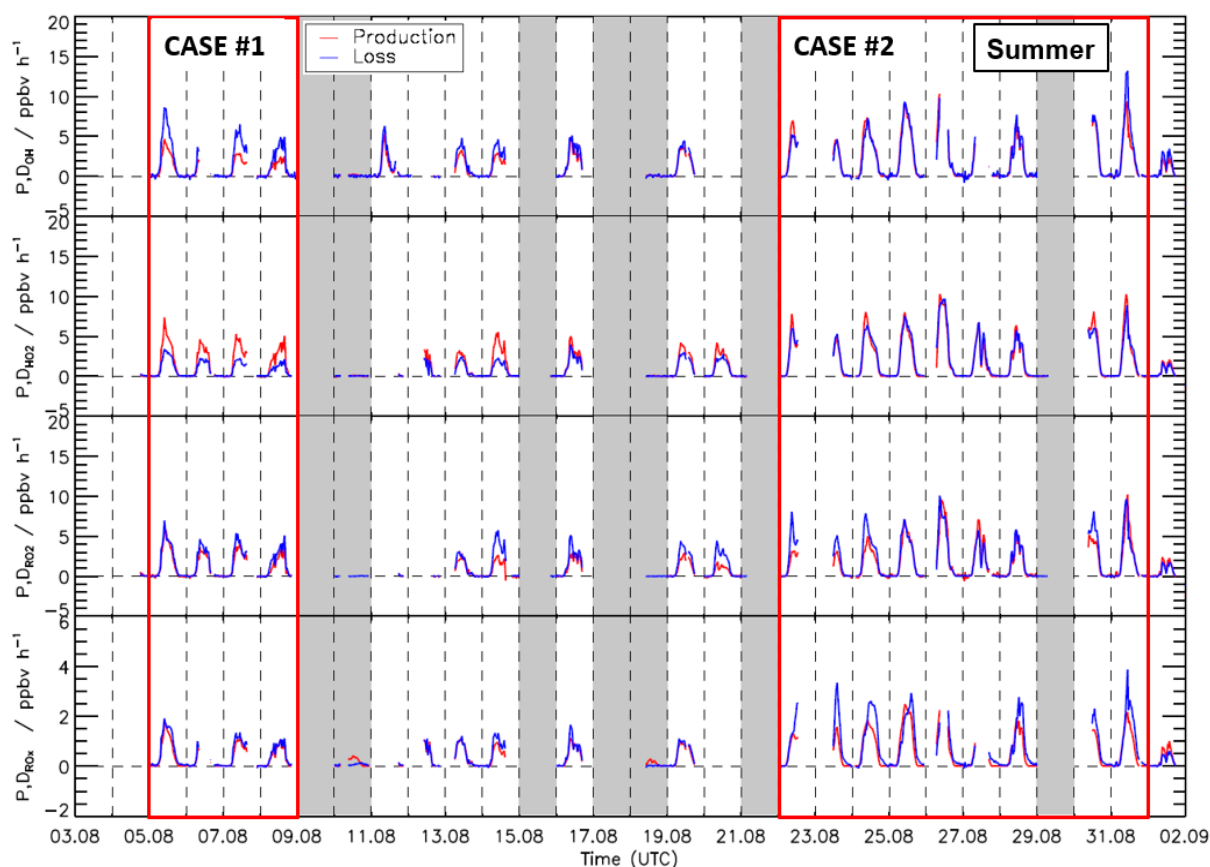


Figure 7: Time series of total production and destruction rates of OH, HO₂, RO₂, and RO_x radicals in the summer period of the JULIAC campaign. Vertical dashed lines denote midnight. Grey areas indicate calibration days and days when the chamber roof was closed. The red boxes denote periods that are discussed in more detail (Case 1 and Case 2).

512 3.5 Chemical budgets of OH, HO₂, RO₂ and RO_x radicals in the spring and summer periods

513 Due to the very low photochemical activity observed in autumn and winter, which resulted in radical
 514 concentrations close to the detection limit of the instrument, the chemical budget analysis is only
 515 discussed for data from the spring and summer periods. It focuses on daytime conditions.

516 Time series of turnover rates of reactions involving OH, HO₂, RO₂ and RO_x radicals in the spring and
 517 summer periods are presented in Fig. 6 and 7, respectively, and median diurnal profiles in Fig. 8. Typical
 518 daytime turnover rates of OH, HO₂ and RO₂ radicals were between 3 ppbv h⁻¹ and 10 ppbv h⁻¹. The rates
 519 of RO_x production and destruction ranged from 1 ppbv hr⁻¹ to 3 ppbv hr⁻¹, which is 2 to 4 times lower
 520 than those of OH, HO₂, and RO₂, because radical conversion reactions cancel out. The highest OH
 521 turnover rate of 13 ppbv h⁻¹ was observed on 31 August, when the air temperature in the chamber reached
 522 up to 40°C. Unusually high turnover rates for HO₂, RO₂, and RO_x radicals occurred on 29 April with

523 values of 14 ppbv h⁻¹, 15 ppbv h⁻¹, and 4 ppbv h⁻¹, respectively, when the NO mixing ratio exceeded 9
524 ppbv. For the reasons stated in Section 3.1, the HO₂ and RO₂ data on this date are considered highly
525 uncertain and were excluded from further analysis of the chemical budgets.

526 Diurnal variations of total radical production and destruction rates, as well as of the contributions of the
527 most important reactions, are shown as median values for the entire spring and summer period in Fig. 8.
528 For OH, the reaction of HO₂ with NO (Reaction R10) was the dominant production pathway contributing
529 more than 70 % to the total production rate in both spring and summer periods. The photolysis of HONO
530 (Reaction R1) was the most important primary OH source during daytime contributing approximately 20 %
531 to the total OH production. The reaction of HO₂ with ozone (Reaction R11), the photolysis of ozone
532 (Reaction R2), and the ozonolysis of alkenes (Reaction R5) contributed less than 3 % to the total OH
533 production. The maximum median total OH production rate of 3.5 ppbv hr⁻¹ was observed in the morning
534 shortly after the peak NO concentration in both spring and summer (Fig. 5). Values gradually decreased
535 until sunset. Median total OH destruction rates were higher than production rates and reached up to 5
536 ppbv hr⁻¹ and 6 ppbv hr⁻¹ at noon in spring and summer, respectively. The contributions of different
537 reactions to the total OH destruction rate is described by the contribution of OH reactants to the OH
538 reactivity (Section 3.4, Fig. 5).

539 Short-lived radicals are expected to be in a steady state, and therefore radical production and destruction
540 rates must be balanced. An imbalance between the calculated rates indicates inaccurate data or a missing
541 radical production or destruction process. The daily peak of the OH production rates was typically lower
542 than the destruction rate by approximately 1.8 ppbv h⁻¹ in the spring and 2.5 ppbv h⁻¹ in the summer period
543 (36 and 43 % of the total OH destruction rate). These discrepancies are higher than the uncertainty of the
544 calculation (Fig. 8).

545 80% of the HO₂ production rate consisted of the reaction of RO₂ with NO (Reaction R9). The remaining
546 part of the HO₂ production rate was due to the photolysis of formaldehyde (9 %) and the reaction of
547 formaldehyde with OH (10 %). Other reactions producing HO₂ played a minor role (< 1 %). The HO₂
548 destruction was mostly due to the reaction of HO₂ with NO (Reaction R10) contributing on average 88 %
549 to the total production rate. The loss due to reaction of HO₂ with RO₂ radicals (Reaction R16) contributed
550 on average 9 % to the total loss.

551 Median values of the total HO₂ destruction and production rates were well balanced in the spring period,
552 with the production rate being slightly higher than the destruction rate. The maximum difference of 1
553 ppbv hr⁻¹, however, was insignificant compared to the uncertainty of the calculation. A similar tendency
554 but more pronounced feature was observed in summer. Here, the median value of production rate was
555 higher than that of the destruction rate by 1.8 ppbv hr⁻¹ (38 % of the total HO₂ production rate) but
556 differences were variable (Fig. 7). This aspect is discussed in more detail for two periods (Sections 3.7
557 and 3.8), which exhibited different degrees of imbalances in the radical budgets.

558 The RO₂ production rate was dominated by the reaction of VOCs with OH (Reaction R8). The
 559 contributions of ozonolysis of measured alkenes to the RO₂ production were very small (less than 1 %).
 560 The reaction of RO₂ with NO (Reaction R9) dominated the RO₂ destruction and contributed more than 90 %
 561 to the total loss rate. In the late afternoon, the RO₂ termination reaction with HO₂ gained in importance

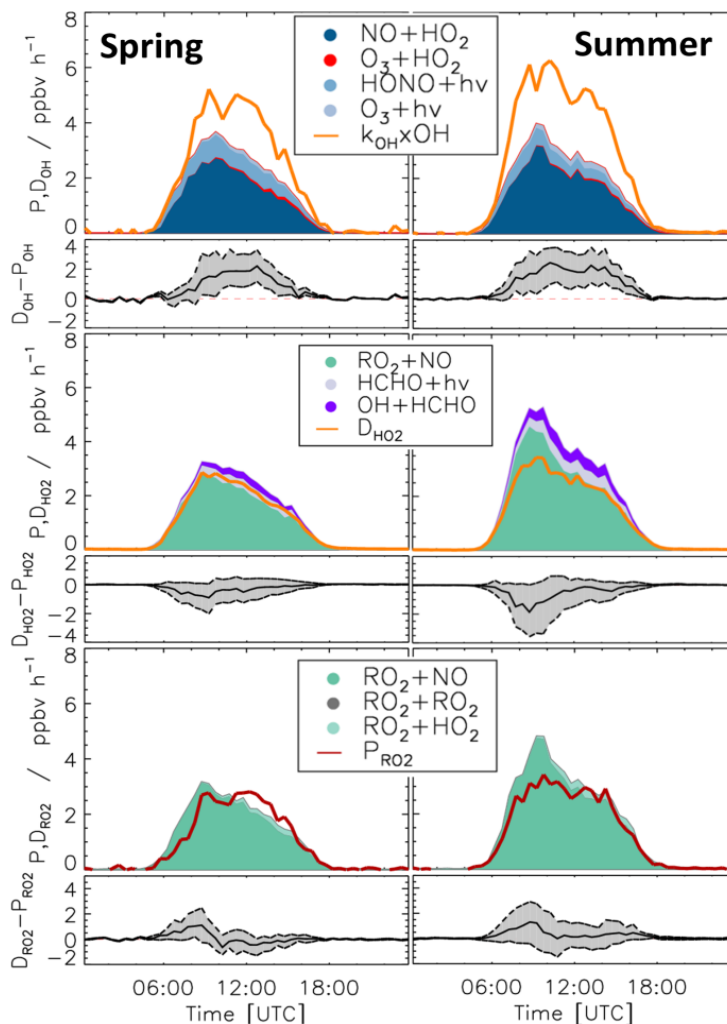


Figure 8: Median values of production and destruction rates of OH, HO₂, and RO₂ radicals in the spring and summer periods of the JULIAC campaign, with data from 29 April excluded. In addition, the differences between the destruction and production rates are shown. Grey areas indicate the 1 σ uncertainty derived from experimental errors of the measured quantities (Table 2) and of the reaction rate constants (Table 1). The reactions that have insignificant contributions to the production or destruction rates are not shown.

562 with contributions of up to 10 %. Although slight imbalances of up to 1 ppbv were observed in the early
 563 morning, the RO₂ production and destruction rates were generally balanced within the uncertainty of
 564 calculations in both spring and summer.

565 Figure 9 shows the calculated RO_x production and destruction rates. The photolysis of HONO (Reaction
 566 R1), HCHO (Reaction R3) and O₃ (Reaction R2) were the dominant processes initiating radical chemistry
 567 and contributed to the total RO_x production rate on average 45 %, 38 % and 15 %, respectively, in both
 568 periods. In the morning, the reaction of OH with NO₂ (Reaction R12) was the most important radical
 569 termination process contributing up to 65 % to the total RO_x destruction rate. In addition, due to relatively
 570 high NO mixing ratios in the early morning, the reactions of OH with NO (Reaction R13) and RO₂ with
 571 NO, which yields organic nitrate (Reaction R14), were also significant radical termination processes
 572 contributing 13 % and 17 % to the total RO_x destruction rate, respectively. In the afternoon, radical self-
 573 reactions (Reaction R15 – R17), and, in particular, the reaction of RO₂ with HO₂ (Reaction R16),
 574 dominated the RO_x destruction due to the low NO and NO₂ mixing ratios. In both periods, spring and
 575 summer, the total RO_x destruction rate was slightly higher than the production rate, in particular, in the
 576 afternoon. The imbalance was up to 0.5 ppbv h⁻¹, which is higher than the uncertainty of the calculations.

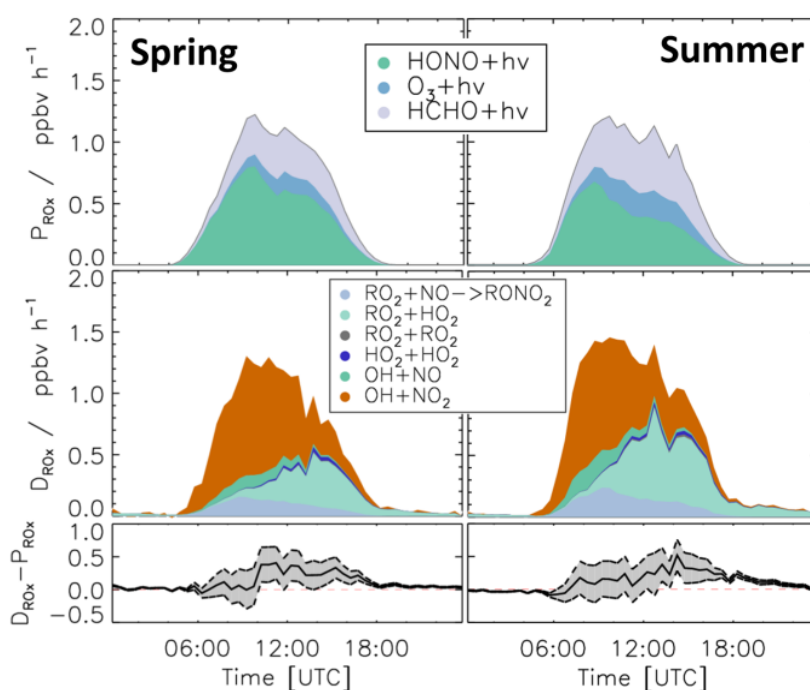


Figure 9: Median values of production and destruction rates of RO_x radicals during the spring and summer periods of the JULIAC campaign. In addition, the differences between the destruction and production rates are shown. Grey areas indicate the 1 σ uncertainty derived from experimental errors of the measured quantities (Table 2) and of the reaction rate constants (Table 1). The reactions that have insignificant contributions to the production or destruction rates are not shown.

577 Meteorological and chemical conditions were variable especially in the summer period causing variations
 578 in the balance between radical production and destruction rates (Fig. 7 and Table S3). In the following,
 579 the chemical budgets with the largest and smallest observed imbalances are discussed: August 5-8 (Case 1)
 580 and August 22-31 (Case 2).

581 3.5.1 Case 1: 5 - 8 August 2019

582 For the period between 5 and 8 August, relatively low NO mixing ratios (maximum: 1 ppbv, median: 0.26
583 ppbv) and typical summer temperature for this region (median: 27°C) were observed (Fig. 10 and Table
584 S3).

585 As for the whole summer period (Fig. 8), the reactions of peroxy radicals with NO (Reaction R9, R10)
586 dominated the inter-radical conversion reactions of OH, HO₂ and RO₂ in this period (Fig. 10). A
587 significant imbalance between the OH production and destruction rates of up to 3.0 ppbv h⁻¹ (51 % of the
588 total OH destruction rate) is found, which cannot be explained by the uncertainty of the calculations. The
589 total HO₂ production rate was 2.0 ppbv h⁻¹ higher than the destruction rate (48 % of the total HO₂
590 production rate), whilst the RO₂ production and destruction rates were well balanced. Relatively small but
591 nevertheless significant differences between RO_x production and destruction rates (0.5 ppbv h⁻¹) were
592 observed during daytime (Fig. 11).

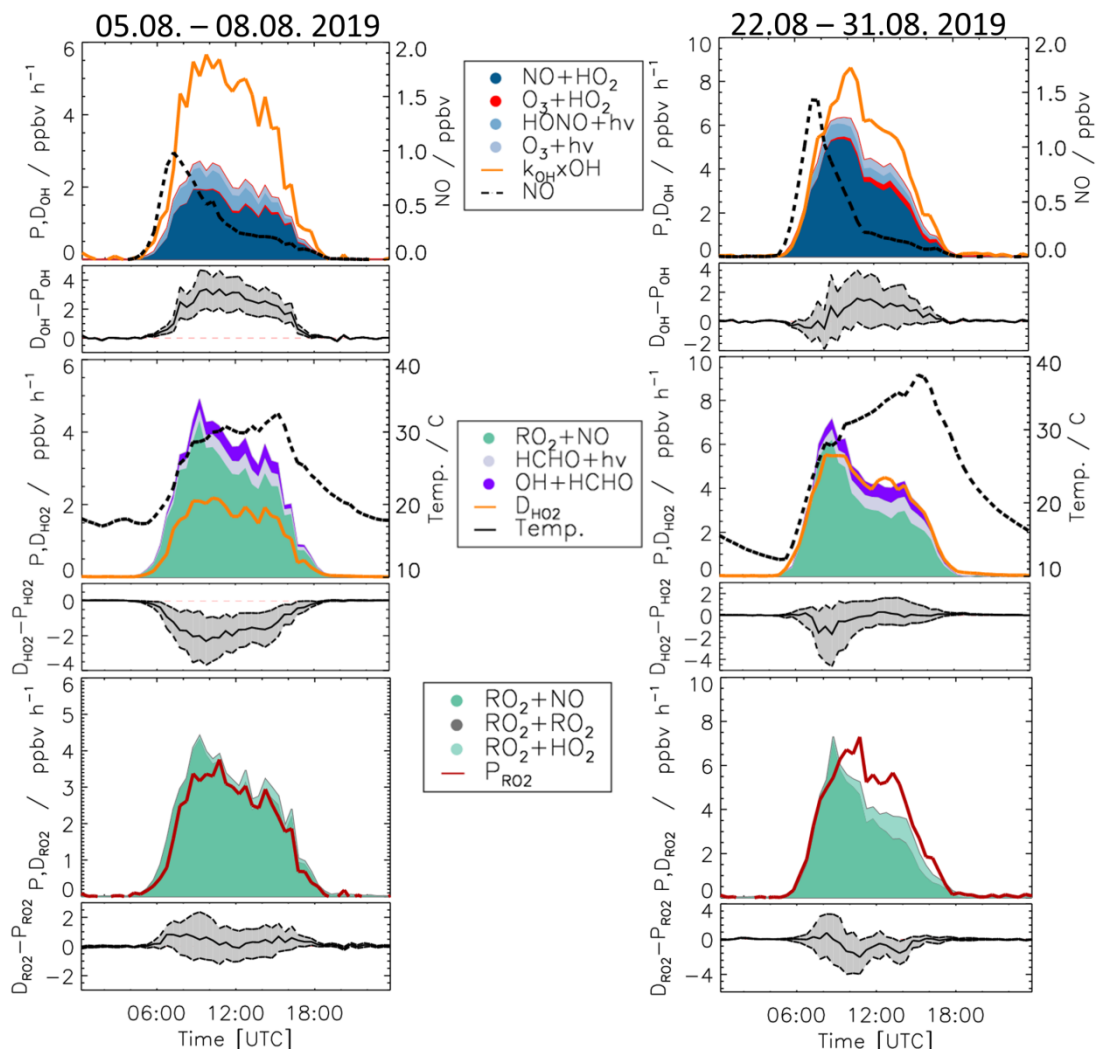


Figure 10: Production and destruction rates of OH, HO₂, and RO₂ radicals for Case 1 (05.08. - 08.08. 2019) and Case 2 (22.08 - 31.08. 2019). In addition, the differences between the destruction and production rates are shown. Grey areas give the 1 σ uncertainty derived from experimental errors of the measured quantities (Table 2) and of the reaction rate constants (Table 1). The reactions that have insignificant contributions to the production or destruction rates are not shown.

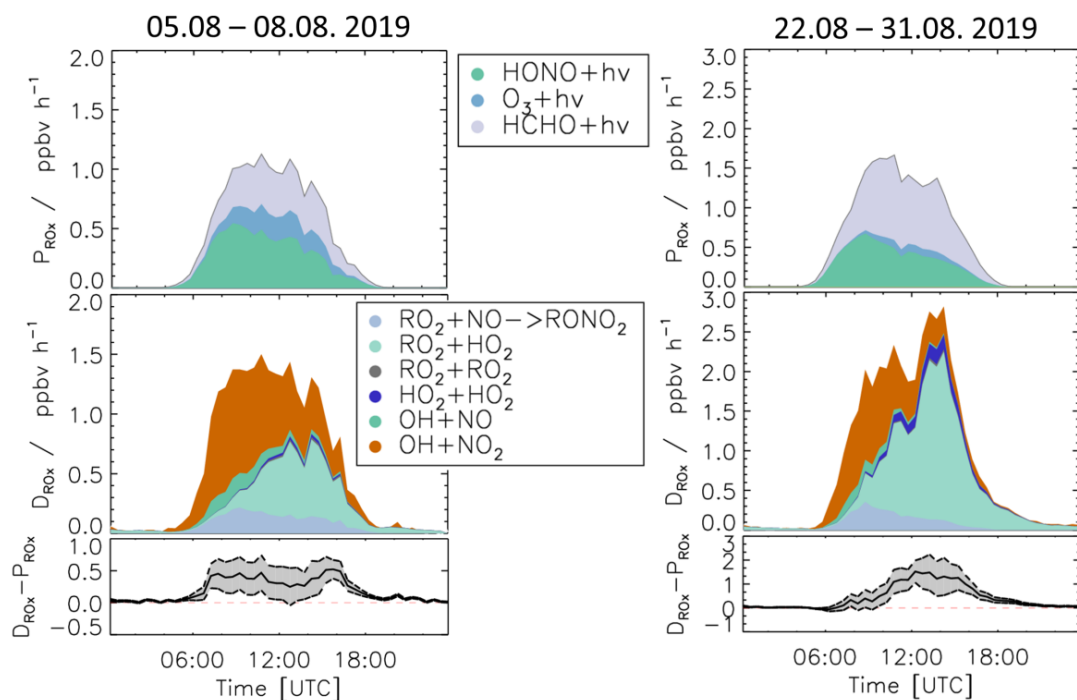


Figure 11: Production and destruction rates of RO_x for the periods of the case studies (Case 1 and Case 2). In addition, the differences between the destruction and production rates are shown. Grey areas indicate the 1σ uncertainty derived from experimental errors of the measured quantities (Table 2) and of the reaction rate constants (Table 1). The reactions that have insignificant contributions to the production or destruction rates are not shown.

594 3.5.2 Case 2: 22 - 31 August 2019

595 During the period from 22 to 31 August, the temperature was generally high and reached a maximum
 596 value of 42°C inside the chamber. The concentrations of radical precursors, HONO, HCHO and O_3 , were
 597 higher than those observed in Case 1 (Table S3). Ozone mixing ratios reached values up to 100 ppbv,
 598 while daytime NO mixing ratios were similar as in Case 1 (<1.5 ppbv, median value of 0.22 ppbv). The
 599 conditions outside the chamber were characterized by stagnant air (wind speed < 4 m/s at 50 m height)
 600 with no precipitation. At these conditions, vigorous biogenic emissions can be expected (Vilà-Guerau de
 601 Arellano et al., 2009; Sarkar et al., 2020). Enhanced biogenic VOC emissions and their photochemical
 602 degradation can therefore explain the higher VOC and HCHO concentrations in Case 2 compared to the
 603 cooler period beginning of the month (Table S3). The larger VOC reactivity and comparable OH
 604 concentrations resulted in HO_2 and RO_2 concentrations that were approximately 2 to 3 times higher than
 605 in Case 1 (Table S3).

606 Imbalances between the radical production and destruction rates were a factor of 2 smaller in the warmer
 607 and more photochemically active period of Case 2 compared to Case 1. OH destruction rates were up to
 608 1.5 ppbv h^{-1} (25 % of the total OH destruction rate) higher than the total production rate (Fig. 10). The
 609 HO_2 production and destruction rates agree within ± 1 ppbv h^{-1} . The contributions from photolysis of

610 HCHO and the reaction of HCHO with OH to the HO₂ production rate were larger compared to other
611 periods with values of up to 15% and 13%, respectively, due to high HCHO mixing ratios of up to 8 ppbv
612 (Fig. 2). The RO₂ production and destruction rates showed imbalances by up to 1.5 ppbv h⁻¹ in the late
613 afternoon.

614 While HONO photolysis was the dominating RO_x source during most of the time in spring and summer
615 (Fig. 9), HO₂ production from the photolysis of HCHO was the most important primary radical source in
616 Case 2 due to the high concentration of HCHO (Fig. 11). Although the chemical budgets for each radical
617 species were essentially closed within the experimental uncertainty, the total loss rate of RO_x was
618 consistently higher than the production rate during daytime. The deviation was higher than the
619 experimental uncertainty and reached a maximum value of 1.4 ppbv h⁻¹ at noontime.

620 **3.5.3 NO dependence of radical production and destruction rates**

621 One of the most influential parameters for the radical chemistry is the concentration of NO, since the
622 reaction with NO dominates the conversion rate of RO₂ to HO₂ (Reaction R10) and HO₂ to OH (Reaction
623 R9) (Fig. 10). Figure 12 shows the NO dependence of median values of the calculated production and
624 destruction rates for the different radicals for the spring and summer period.

625 For OH, the production rates are consistently lower than the destruction rates by about 1.5 ppbv h⁻¹ for
626 NO mixing ratios lower than 1 ppbv NO. At higher NO, the OH budget is balanced within the
627 experimental uncertainty. For HO₂, an inverse pattern is observed. Below 1 ppbv NO, the production rate
628 is higher than the destruction rate by about 1 ppbv h⁻¹. Only for lowest NO mixing ratios, the production
629 and destruction rates are balanced. For NO mixing ratios above 1 ppbv, the chemical budget of HO₂ is
630 essentially closed. For NO mixing ratios of 3.5 ppbv, the difference between production and destruction
631 rate is noticeably high with 4 ppbv h⁻¹ but has also a large uncertainty. For RO₂ radicals, the chemical
632 budget is closed for NO mixing ratios below 1 ppbv but an increasing discrepancy between the loss and
633 production rates is observed with increasing NO mixing ratios. While the production rate is relatively
634 constant with a value of 2.5 ppbv h⁻¹, the loss rate increases to values of up to 7.5 ppbv h⁻¹ at 3.5 ppbv NO.
635 The budget of RO_x, in which radical inter-conversion reactions cancel out, is mostly balanced over the
636 whole range of NO. Only for lowest and highest NO mixing ratios the destruction rate is 0.6 ppbv h⁻¹
637 higher than the production rate.

638

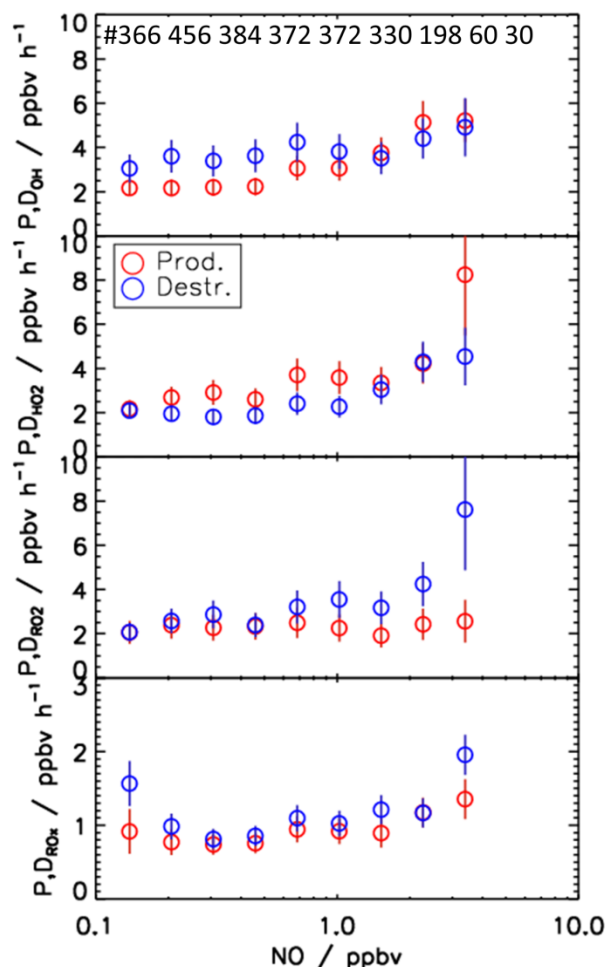


Figure 12: NO dependence of median production and destruction rates of OH, HO₂, RO₂, and RO_x radicals. Median values include all data from the spring and summer periods of the JULIAC campaign (NO intervals: ln(NO) = 0.4 ppbv). Vertical bars represent the 1σ uncertainty from experimental errors of the measured quantities (Table 2) and of the reaction rate constants (Table 1). The number of data points in each NO bin is represented on the top panel.

639

640 4 Discussion

641 4.1 Discrepancies in the chemical budgets of radicals

642 The highest imbalances in the chemical budgets of radicals are found for OH radicals. In spring and
 643 summer, their production rate was consistently lower than the loss rate (Fig. 8). This deficit was largest
 644 beginning of August (Case 1, Fig. 10) when the discrepancy reached (3.0 ± 1) ppbv h⁻¹.

645 Imbalances in the radical budgets can be observed for different reasons. They can be caused by missing
 646 processes or incorrect rate constants in the calculations of the production or destruction rates (Section 4.2).
 647 It is also possible that measured concentrations that are used for the calculation contain unknown errors.

648 The technically difficult radical measurements have a large potential for artefacts (Hofzumahaus and
649 Heard, 2016). Precautions were taken to minimize measurement interferences for OH and HO₂ in this
650 campaign:

- 651 • The measurements of OH by the LIF instrument were interference-corrected using chemical
652 modulation and agreed with simultaneous OH measurements by the DOAS instrument within the
653 experimental uncertainties. The measured OH reactivity quantifies the total chemical loss rate of
654 OH caused by atmospheric reactants and has a total accuracy of 10%. Thus, the destruction rate
655 of OH, which is the product of the concentration and reactivity of OH, is known within 20 % and
656 is unlikely biased by unknown OH interferences or unknown atmospheric reactants.
- 657 • The O_x production rate calculated from the reaction of peroxy radicals with NO agrees with the
658 measured increase of O_x concentrations within ±1 ppbv h⁻¹ for most conditions (Section 3.1). As
659 more than 70 % of the OH production is due to the reaction of HO₂ with NO (Reaction R10), a
660 bias of more than 1 ppbv h⁻¹ due to an unaccounted HO₂ measurement error seems unlikely.
- 661 • The analysis of the chemical budget of OH in previous chamber experiments performed at
662 various chemical conditions showed no evidence for a missing OH source originating from
663 chamber wall effects (Kaminski et al., 2017; Fuchs et al., 2018; Novelli et al., 2018; Rolletter et
664 al., 2019; Rolletter et al., 2020).

665 Thus, there is no evidence for instrumental errors that are not included in the estimated errors of the
666 calculated turnover rates. The observed imbalances in the OH budget of up to 3 ppbv h⁻¹ are therefore
667 most likely due to a missing OH source.

668 The missing OH production is correlated with the imbalance in the HO₂ budget, for which the production
669 rate is larger than the loss rate at low NO mixing ratios (Fig. 12). This is most clearly seen in the period of
670 Case 1, when the discrepancy reaches (2.0±1) ppbv h⁻¹ (Fig. 10). The production rate of HO₂ is nearly
671 equal to the RO₂ loss rate ($P_{HO_2} \approx D_{RO_2}$) because both are controlled by the reaction of RO₂ with NO
672 (Reaction R9). Furthermore, the RO₂ loss rate is well balanced by the RO₂ production rate within the
673 experimental uncertainty of ±1 ppbv h⁻¹ (Fig. 8 and 10). Thus, there is no hint that the calculated turnover
674 rate of the RO₂ + NO reaction had a bias higher than 1 ppbv h⁻¹. In addition, turnover rates of the
675 reactions of HO₂ and RO₂ with NO producing ozone are consistent with the observed O_x increase in the
676 chamber (Section 3.1). This suggests that these rates are correct in the chemical budget analysis. For the
677 above reasons, the discrepancy between HO₂ production and destruction rates is most likely due to a
678 missing HO₂ loss process and not by measurement errors of HO₂, RO₂ or NO.

679 RO_x destruction rates are generally higher than the production rates but differences are on average lower
680 than 0.5 ppbv h⁻¹ (Fig. 9). In the periods of Case 1 and Case 2, the corresponding discrepancies reach 0.5
681 ppbv h⁻¹ and 1.4 ppbv h⁻¹, respectively (Fig. 10). If these discrepancies were due to a missing primary OH
682 source, they could also explain a small part (17 %) of the imbalance in the chemical OH budget in Case 1,
683 and the complete imbalance in the OH budget in Case 2.

684 It is difficult to identify the exact cause for the differences in OH and HO₂ budgets observed for Case 1
685 and 2 only with the available data. Case 2 was characterized by high temperature with increased BVOC
686 emissions and high levels of HCHO (Table S3). No clear correlation was found between the ratio of the
687 production and destruction rates of the radicals and the concentration of chemical species such as NO,
688 NO₂, O₃, HCHO, etc. A weak correlation was observed with temperature with an improved balance in the

689 budgets the higher the temperature was. This could indicate that the unaccounted processes become less
690 competitive for high radical turnover rates with chemical conditions being dominated by organic
691 compounds from biogenic emissions.

692 In conclusion, the radical budget analysis suggests the presence of a missing OH source and a missing
693 HO₂ loss process with a similar turnover rate at NO mixing ratios below 1 ppbv for typical temperatures
694 in summer. The opposing imbalances in the OH and HO₂ budgets could be due to an unknown
695 mechanism that converts HO₂ to OH, or they could indicate a missing primary OH source and a similar
696 fast, but independent termination reaction removing HO₂. The remaining imbalance in the RO_x budget
697 would be consistent with an unaccounted primary OH source. This fits best the observations in Case 2
698 characterized by high temperatures and VOC emissions.

699 For NO mixing ratios that are higher than 1 ppbv, production and destruction rates of OH and HO₂
700 radicals are generally balanced (Fig. 12). An exception is observed for HO₂ for highest NO mixing ratios
701 of 3.5 ppbv, for which the production rate is 3.5 ppbv h⁻¹ higher than the loss rate.

702 For RO₂, the radical budget is not closed, but the loss rate increases with NO in contrast to the production
703 rate. The difference reaches a value of 5 ppbv h⁻¹ at 3.5 ppbv NO. In the same range of NO mixing ratios,
704 the odd oxygen production rate (P_{O_x}) calculated by peroxy radicals (Eq. 14) overestimates the observed
705 increase in the O_x mixing ratio by about 3 ppbv h⁻¹. This difference points to a systematic error in the
706 peroxy radical measurements explaining a considerable part of the imbalance in the RO₂ budget. A
707 reduction of the RO₂ concentration by 3×10^7 cm⁻³ would reduce the HO₂ production rate by 3 ppbv h⁻¹
708 and resolve the discrepancy in the odd oxygen production calculations for the highest NO mixing ratio.
709 The presumed bias in the RO₂ measurement may be caused by an incorrect background subtraction that
710 becomes most relevant at high NO concentrations (Section 3.1). However, even after correction of this
711 bias a discrepancy in the RO₂ budget would remain requiring an additional RO₂ source of approximately
712 2 ppbv h⁻¹ to be balanced.

713 Further information on the nature of the missing RO₂ source can be obtained from the chemical budget of
714 RO_x, for which the production rate is 0.5 ppbv h⁻¹ smaller than the loss rate at 3.5 ppbv NO (Fig. 12).
715 This discrepancy cannot be explained by the instrumental uncertainties in HO₂ and RO₂ measurements,
716 because the RO_x budget at high NO in the morning was dominated by OH reactions with NO₂ and (Fig.
717 9). Thus, the imbalance in the RO_x budget at high NO indicates a missing primary radical source, which
718 on a single day (29 April) even reached 3 ppbv hr⁻¹ (Fig. 6). As the OH budget is balanced for most of
719 the time and the corresponding HO₂ budget does not require an additional HO₂ source, a missing primary
720 RO₂ source is a likely explanation for the discrepancy in the RO_x budget. This would also explain part of
721 the imbalance in the RO₂ budget at high NO concentrations.

722

723 4.2 Potentially missing chemical processes

724 The above discussion shows that imbalances between calculated production and destruction rates are
725 highly variable over time and change with chemical conditions. As main general features in spring and
726 summer, the radical budget analysis indicates unaccounted OH production processes with a typical
727 strength of 1.5 – 3 ppbv h⁻¹ at low NO concentrations, which coincides with a missing HO₂ sink of 1 – 2

728 ppbv h⁻¹. At high NO mixing ratios (> 1 ppbv), the radical budgets for OH and HO₂ radicals are relatively
729 well balanced, but RO₂ production processes of about 2 ppbv h⁻¹ appear to be missing in the RO₂ radical
730 budget. In the following, potential reasons for the observed discrepancies in the radical budgets are
731 discussed.

732 **4.2.1 Differences in the chemical behavior of specific RO₂ radicals**

733 As no speciated RO₂ radicals were detected but the sum of all RO₂ species, effective rate coefficients for the
734 reaction of all RO₂ species with NO (Reaction R9, R14), RO₂ (Reaction R15), and HO₂ (Reaction R16)
735 are used from structure-activity relationship (SAR) by Jenkin et al. (2019) for the calculations of turnover
736 rates. Potential systematic errors due to this simplification for reactions of RO₂ with RO₂ and HO₂ are
737 expected to be negligible due to their small contributions to the total turnover rates.

738 In contrast, the reaction of RO₂ with NO plays an important role in the chemical budgets of HO₂ and RO₂.
739 The reaction has one channel that converts RO₂ to HO₂ (Reaction R9) and one radical termination channel
740 that produces organic nitrates (RONO₂) (Reaction R14). The unknown speciation of RO₂ causes
741 uncertainty with respect to the total rate constant of the RO₂ + NO reaction ($k_9 + k_{14}$). An effective value
742 of $9 \times 10^{-12} \text{ cm}^3 \text{ s}^{-1}$ was taken from (Jenkin et al., 2019). A high limit for the total rate coefficient of
743 RO₂ + NO (for example $1.1 \times 10^{-11} \text{ cm}^3 \text{ s}^{-1}$, 298K for c-C₅H₉O₂) would slightly increase the imbalances
744 between production and destruction rates for HO₂ and RO₂ radicals by 13 % for both spring and summer.
745 A lower limit would be the rate constant of the reaction of methyl peroxy radicals (CH₃O₂) with NO
746 having a value of $7.7 \times 10^{-12} \text{ cm}^3 \text{ s}^{-1}$ (298 K)., Applying this number in the calculations for HO₂
747 production and RO₂ destruction rates (Fig. S6) for the period when observed discrepancies in the HO₂
748 budget were highest (Case 1) further improves the already well balanced budget of RO₂ radicals. This
749 also reduces the imbalance between HO₂ destruction and destruction rates, but the effect is rather small
750 (approximately 10%) and not sufficient to explain the total difference. For the other periods such as the
751 spring period and the period of Case 2, a reduced reaction rate would worsen the observed imbalances.

752 An additional uncertainty in the HO₂ production rate comes from the assumed yield of organic nitrates in
753 the reaction of RO₂ with NO. Typical organic nitrate yields range from 5 % to 20 % (Jenkin et al., 2019).
754 The low limit value is applied in the calculations above. Using a value of 20 % decreases the discrepancy
755 between HO₂ production and destruction rates from 2.0 to 1.5 ppbv h⁻¹ for the period of Case 1.

756 It is worth noting that the organic nitrate yield is generally higher for larger hydrocarbons, but the rate
757 constant for the RO₂ + NO reaction is also often higher, so that there are compensating effects in the
758 production efficiency of HO₂. In addition, it is expected that only a fraction of RO₂ radicals is produced
759 from large hydrocarbons due to the major composition of RO₂ would be methyl peroxy radicals.

760 For the above reasons, the unknown speciation of RO₂ is unlikely the reason for the observed imbalances
761 in the HO₂ budget that are most prominent in the period of Case 1.

762 **4.2.2 Unaccounted primary radical sources**

763 Primary RO_x radical production that may not be appropriately accounted for in the calculations could be
764 OH, HO₂, and RO₂ production from the ozonolysis of alkenes. Only few alkene compounds were
765 measured in the JULIAC campaign. The contribution from the ozonolysis of these alkenes to the radical
766 production was very small with values in the range of 0.005 to 0.03 ppbv h⁻¹ (Section 3.5). The ozonolysis

767 of small alkenes such as propene and cis-2-butene that were not measured but are often abundant for
768 example in forested areas (Goldstein et al., 1996; Rhew et al., 2017), may have significantly contributed
769 to the radical production.

770 The potential impact of unmeasured alkenes on the primary radical production is tested by assuming that
771 the OH reactivity that cannot be explained by measured OH reactants (on average, 2.5 s^{-1}) originates from
772 1.5 ppbv propene and 1.0 ppbv cis-2-butene. The radical production by ozonolysis of the additional
773 propene and cis-2-butene increases the production from ozonolysis of measured species by more than an
774 order of magnitude in both spring and summer periods of the JULIAC campaign (Fig. S7) The
775 discrepancies between the total RO_x production and destruction rates is significantly decreased for the
776 period of the 2 Case studies by approximately 0.2 ppbv h^{-1} . However, the additional OH production is by
777 far insufficient to explain the missing OH source that was generally found during the JULIAC campaign.
778 In addition, the corresponding OH and O_3 reactivity from the additional alkene compounds is about a
779 factor of 6 larger than of alkenes (e.g., ethene, propene, trans-2-butene, cis-2-pentene) that were measured
780 in ambient air next to the SAPHIR chamber in the HOxComp campaign in July 2005 (Elshorbany et al.,
781 2012; Kanaya et al., 2012).

782 The photolysis of oxygenated organic compounds is another source for radicals that could be
783 underestimated in the calculations. Only the photolysis of HCHO is included in the production rate of
784 HO_2 and RO_x at all times of the campaign. In addition, acetaldehyde (CH_3CHO), methyl vinyl ketone
785 (MVK), methacrolein (MACR), and methylglyoxal were measured during part of the campaign and were
786 not included in the analysis in Section 3. Calculations show that radical production rate from their
787 photolysis was less than 0.1 ppbv h^{-1} . Thus, photolysis of unmeasured OVOCs was very likely
788 unimportant in the present study. This is consistent with similar small contributions from photolysis of
789 OVOCs other than HCHO found in in the HOxComp campaign (Kanaya et al., 2012). In addition, during
790 the HOxCOMP campaign the modelled OH reactivity could be matched with the measured reactivity by
791 including either additional primary emissions (Kanaya et al., 2012) or model-produced oxygenated
792 secondary products (Elshorbany et al., 2012). Neither of the additional species contributed enough to
793 close the radical budgets. If it is assumed that the missing OH reactivity (2.5 s^{-1}) is all due to glyoxal (9
794 ppb) an additional OH production of 0.3 ppbv h^{-1} could be expected. This would still not be enough to
795 close the radical budget suggesting that unmeasured OVOCs do not play a large role.

796 The photolysis of ClNO_2 constitutes a primary radical source (Reaction R20, R22) that can be found in
797 coastal environments (e.g., Osthoff et al. (2008)) and mid-continental regions (e.g., Thornton et al.
798 (2010)). The availability of ClNO_2 data during the summer period allowed assessing the potential impact
799 of its photolysis on the RO_2 radical production (Eq. 9). Due to the low mixing ratio of ClNO_2 of less than
800 0.4 ppbv (Tan et al., 2022), the RO_2 production from Cl oxidation processes was insignificant ($<0.1 \text{ ppbv}$
801 h^{-1}) and cannot explain the observed discrepancies in the primary production and destruction rates of
802 radicals in the summer period and in the case studies. The instrument detecting ClNO_2 was not available
803 in the spring period of the campaign. Therefore, the extent to which ClNO_2 photolysis contributed in
804 spring, for example to the large missing RO_x source (up to 3 ppbv hr^{-1}) on 29 April, remains unknown.

805 **4.2.3 Unaccounted radical termination reactions**

806 Heterogeneous uptake of HO_2 on aerosol is a potential termination reaction that is not included in the HO_2
807 and RO_x destruction rates above. However, the impact of including the heterogeneous HO_2 loss on

808 aerosol surface (Eq. 8) on the total loss rate is insignificant (less than 1 %), even if a high effective uptake
809 coefficient of 0.2 is assumed (Fig. S7).

810 As HO₂ uptake is a radical termination process, its relative contribution to the total RO_x loss rate can be
811 higher compared to the relative contribution to the total HO₂ loss rate. However, the only notable
812 influence would be for the period of Case 2 (8 % of total RO_x loss rate), when the aerosol surface area
813 concentration was high with values of up to $3.0 \times 10^2 \mu\text{m}^2 \text{cm}^{-3}$.

814 The estimate for the heterogeneous HO₂ loss rate has a high uncertainty because the uptake coefficient
815 highly depends on the aerosol properties that were not fully characterized in this campaign. Previous
816 laboratory investigations showed a large variability for the uptake coefficient with values ranging from
817 0.08 to 0.6 depending on the aerosol chemical composition and the physical state (George et al., 2007;
818 Taketani et al., 2008, 2009; George et al., 2013; Lakey et al., 2015; Song et al., 2020; Tan et al., 2020).
819 Even the largest reported HO₂ uptake coefficients cannot explain the observed differences in the chemical
820 budget of HO₂ radicals. Therefore, heterogeneous HO₂ reactions can be ruled out as an explanation for the
821 unexplained HO₂ loss rate.

822 **4.2.4 Unaccounted radical inter-conversion reactions**

823 In the last decade, it has been discovered that unimolecular reactions of RO₂ can significantly increase
824 atmospheric OH concentrations in low-NO environments where they can compete with the reaction of
825 RO₂ with NO. The most important, atmospherically relevant example is the production of OH from the
826 isomerization of isoprene-RO₂ radicals (Peeters et al., 2009; da Silva et al., 2010; Peeters and Müller,
827 2010; Crouse et al., 2011; Fuchs et al., 2013; Peeters et al., 2014; Teng et al., 2017; Novelli et al., 2020).
828 The SAPHIR chamber is surrounded by a deciduous forest that emits isoprene especially in summer.
829 Compared to previous campaigns on the campus where up to several ppbv of isoprene were measured
830 (Komenda et al., 2003; Spirig et al., 2005; Kanaya et al., 2012), concentrations were relatively low during
831 the JULIAC campaign (< 0.4 ppbv, on average).

832 The effect of the conversion of RO₂ to OH by the isomerization of isoprene-RO₂ (Eq. 4) is tested in the
833 analysis of the OH and RO₂ budgets. In the afternoon of days in the spring period and the period of Case
834 2, the total OH production increases only 1 % due to the low isoprene mixing ratios (< 0.2 ppbv) and the
835 competition of unimolecular reactions with bimolecular reactions of RO₂ with NO. Even in the summer
836 period, when isoprene mixing ratios were up to 0.8 ppbv, the contribution of isomerization reactions from
837 isoprene-RO₂ radicals to the total turnover rate of RO₂ is still small with values of less than 4 %. This
838 implies that unimolecular decomposition reactions of isoprene-RO₂ radicals made a minor contribution to
839 the RO₂ destruction and OH production rates.

840 Another known isomerization process that produces OH applies to RO₂ that are formed by OH oxidation
841 of methacrolein (MACR) (Crouse et al., 2012; Fuchs et al., 2014), which is an oxidation product of
842 isoprene. MACR mixing ratios were up to 0.5 ppbv in the JULIAC campaign. Because the rate constant
843 for the OH reaction of MACR is smaller than for isoprene, OH regeneration from MACR-RO₂ radicals is
844 even less important than from isoprene-RO₂.

845 For acyl and carbonyl peroxy radicals it was shown that the reaction of RO₂ with HO₂, which mainly
846 forms hydroperoxides (ROOH) (Reaction R16), can produce OH with yields up to 80% (Hasson et al.,

2004; Dillon and Crowley, 2008; Groß et al., 2014; Praske et al., 2015; Winiberg et al., 2016; Fuchs et al., 2018; Jenkin et al., 2019). It is also noteworthy that the rate constant for the reaction of HO₂ with this class of RO₂ species is almost a factor of 2 higher than for other RO₂ species (Jenkin et al., 2019). However, even if it is assumed that all the measured RO₂ are acyl and carbonyl peroxy radicals, the formation of OH from their reaction with NO could only explain up to 0.5 ppbv h⁻¹ of the imbalances in both OH and HO₂ budgets.

Studies in the remote marine boundary layer show that HO₂ to OH conversion mediated by halogen oxides (XO, X = Cl, Br, I) (e.g., Bloss et al. (2005); Sommariva et al. (2006); Kanaya et al. (2007); Stone et al. (2018); Fan and Li (2022)) can significantly contribute to the interconversion of radicals and destroy ozone:



This conversion mechanism would only be effective at low NO, when the consumption of XO by NO (Reaction R25) is comparatively slow and when X is not depleted by other reactions as in the case of Cl by reactions with VOCs (Reaction R22).

For BrO, the rate constants for Reaction R23 and R25 are about the same ($2.1 \times 10^{-11} \text{ cm}^3 \text{ s}^{-1}$ at 298 K, (J. B. Burkholder, 2019)). Thus, the reaction of BrO with HO₂ would only be dominant, if the NO concentration were smaller than the concentration of HO₂, i.e., less than 10 pptv in this campaign. For IO, the situation is similar and NO mixing ratios would need to be less than 40 pptv. Such low NO mixing ratios were not observed during daytime and rule out significant halogen oxide mediated HO₂ to OH conversion. The required XO concentrations to achieve an HO₂ loss rate of 1 ppbv h⁻¹ at an HO₂ concentration of $2 \times 10^8 \text{ cm}^3$ would be 66 pptv BrO or 16 pptv IO, which exceeds the abundances reported for marine environments, where halogen sources are known to exist, by more than an order of magnitude. For these reasons, halogen oxide chemistry cannot explain the missing HO₂ sink and missing OH source in this study.

4.3 Comparison with results from other field campaigns

Although the chemical and physical conditions were partly influenced by the chamber properties (Section 2.1), the radical concentrations observed during spring and summer were within the range of values that have been observed in other field studies in summertime in urban and suburban areas (Tan et al., 2001; Ren et al., 2003; Kanaya et al., 2007; Mao et al., 2010; Lu et al., 2013; Brune et al., 2016; Tan et al., 2017; Whalley et al., 2018; Tan et al., 2019). The impact of the decreased solar radiation by the chamber transmission on the radical production was compensated by the radical production from the photolysis of HONO and HCHO emitted from the chamber film.

This effect is also shown in the relationship between the OH concentration and the photolysis frequencies of ozone, $j_{\text{O}_3^1\text{D}}$ (Section 3.4). The slope ($8.0 \times 10^{11} \text{ cm}^{-3} \text{ s}^{-1}$) of the correlation for the data from the

884 JULIAC campaign is much higher than obtained for data in other field campaigns in similar environments
885 (Ehhalt and Rohrer, 2000; Handisides et al., 2003; Holland et al., 2003; Tan et al., 2017) due to the high
886 OH production by the photolysis of chamber-produced HONO (Reaction R1). This is further confirmed
887 by the similarity in OH and HO₂ radical concentrations between this campaign and what was observed in
888 the HO_xComp campaign when measurements were performed in front of the SAPHIR chamber for 3 days
889 in July 2005 (Elshorbany et al., 2012).

890 In contrast, daytime OH concentrations observed during winter and autumn in the JULIAC campaign
891 were lower than OH concentrations observed in previous wintertime field campaigns (Heard et al., 2004;
892 Ren et al., 2006; Kanaya et al., 2007; Tan et al., 2018; Ma et al., 2019). This is due to the lower photolysis
893 frequencies in the chamber compared to outdoors, which is not compensated by chamber-produced HONO
894 in wintertime, because the emission strength is low at low temperature and low solar radiation.

895 Very low nighttime OH concentration in all seasons of the JULIAC campaign (Section 3.4) is consistent
896 with observations in previous field campaigns in rural areas in Germany (Ehhalt and Rohrer, 2000;
897 Handisides et al., 2003; Holland et al., 2003), in which nighttime OH concentrations were less than $1 \times$
898 10^5 cm^{-3} . However, in several other field studies performed in urban areas, nighttime OH concentrations
899 were in the range of 0.2 to $3 \times 10^6 \text{ cm}^{-3}$, for example in China (Lu et al., 2014; Rohrer et al., 2014; Tan
900 et al., 2017; Tan et al., 2018; Ma et al., 2019; Tan et al., 2019; Wang et al., 2019; Whalley et al., 2021), in
901 the US (Martinez et al., 2003; Brune et al., 2016; Griffith et al., 2016), and in the UK (Ren et al., 2003;
902 Vaughan et al., 2012). In these studies, the high nighttime OH concentrations could not be explained by
903 model predictions and raised questions about the presence of potential interferences in nighttime OH
904 signals measured by LIF instruments (Mao et al., 2012; Lu et al., 2014; Novelli et al., 2014).

905 Similar studies investigating the chemical budgets of OH, HO₂, RO₂, and RO_x radicals like in this study
906 have been performed for data from field campaigns in a suburban area in the Pearl River Delta (PRD),
907 China, in autumn 2014 (Tan et al., 2019), and in central Beijing, China, (Whalley et al., 2021) in summer
908 2017.

909 Tan et al. (2019) observed median values of turnover rates of OH, HO₂ and RO₂ radicals ranging from 10
910 to 15 ppbv h⁻¹, while rates for RO_x initiation and termination rates were on the order of 3 to 4 ppbv h⁻¹
911 during daytime for chemical conditions affected by anthropogenic emissions. From the comparison
912 between the radical production and destruction rates, a missing OH source and a missing RO₂ sink with a
913 similar rate up to 7 ppbv h⁻¹ (45 % of the total OH turnover) were found at low NO mixing ratios below 1
914 ppbv, while HO₂ production and destruction rates were balanced. The authors suggested that an additional
915 chemical mechanism is required that efficiently converts RO₂ to OH without the involvement of NO. One
916 possibility proposed by Tan et al. (2019) is that HO_x radicals are formed from the auto-oxidation of
917 specific RO₂ species which include multifunctional groups such as -OH, -OOH, or -CHO groups.

918 The analysis of the chemical budget of OH radicals in the JULIAC campaign shows that an unaccounted
919 OH source with a rate ranging between 2 and 3 ppbv h⁻¹ (about 50 % of the total OH destruction rate) is
920 required at low NO mixing ratios to balance OH production and destruction rates. This rate is smaller than
921 the rate determined in Tan et al. (2019). However, considering that the OH radical turnover rates in the
922 JULIAC campaign were about half compared to values in the campaign in the PRD area, the relative
923 importance of the unaccounted OH source was comparable in both campaigns. However, the mechanism
924 suggested by Tan et al. (2019) is likely not the only explanation for discrepancies in the radical budgets

925 observed in this study. In the JULIAC campaign, to balance the budget of RO₂ radicals rather requires an
926 additional radical source than additional loss processes particularly at high NO mixing ratios above 1
927 ppbv, and the missing OH sources are likely originating from an HO₂ to OH conversion process and/or a
928 missing primary OH source.

929 Whalley et al. (2021) also investigated the chemical budgets for radicals over a wide range of NO mixing
930 ratios (0.1 to 104 ppbv) from measurement performed in central Beijing, China. Compared to the results
931 in Tan et al. (2019) and to results in this study, the rates of RO_x initiation and termination reactions were
932 2 to 4 times higher. Also, the rates of radical propagation reactions for OH, HO₂ and RO₂ radicals were 5
933 to 10 times higher due to fast inter-radical conversion reactions at conditions with high concentrations of
934 NO. Similar to the results in this study, an OH source with a high rate of up to 15 ppbv h⁻¹ (50 % of the
935 total OH destruction) was required to balance OH production and destruction rates for low NO mixing
936 ratios. This unaccounted OH source is more than 3 times higher than that determined in the JULIAC
937 campaign and in the campaign in China reported by Tan et al. (2019). The HO₂ production rate observed
938 in Beijing largely exceeded the destruction rate by 3 to 5 times for low NO mixing ratios. In contrast,
939 production and destruction of RO₂ and RO_x radicals were well balanced. On the other hand, results for
940 conditions of low NO concentrations, production and destruction of OH radicals were balanced at high
941 NO mixing ratios, while very high imbalances of up to 50 ppbv h⁻¹ were observed for HO₂ and RO₂
942 radicals. Whalley et al. (2021) showed that reducing the rate constant of the reaction between RO₂ and
943 NO by a factor of 10 could close the gaps between production and destruction rates. The authors
944 suggested that the presence of a significant fraction of RO₂ radicals from the oxidation of large and
945 multifunctional VOCs such as monoterpenes and long-chain alkanes could explain observations. These
946 radicals can undergo multiple RO₂ to RO₂ conversion reactions by unimolecular isomerization of alkoxy
947 radicals (RO), which are formed from the reaction of RO₂ with NO, so that no HO₂ is produced. Such a
948 RO₂ radical reaction chain would be equivalent to an increased chemical lifetime of RO₂ radicals, if RO₂
949 species cannot be distinguished by instruments like in the sum measurements performed by RO_x-LIF
950 instruments. Whalley et al. (2021) showed that RO₂ production by this mechanism would largely
951 reconcile discrepancies between modelled and measured RO₂ concentrations (the model-measurement
952 ratio decreases from 6.2 to 1.8), if the OH reactivity that could not be accounted for by measured OH
953 reactants is attributed to α -pinene.

954 Applying a reduced rate constant for RO₂ to HO₂ propagation reactions as suggested in Whalley et al.
955 (2021) in the calculations in this study could help explaining the observed discrepancies between HO₂ and
956 RO₂ production and destruction rates. The largest effect is expected when high NO mixing ratios up to 10
957 ppbv like on 29 April is experienced. In this case, a high reduction of the rate constant by a factor of 2 for
958 all measured RO₂ would be required to close the observed gaps between production and destruction rates.
959 Reduced reaction rate constants of the RO₂+NO reaction could be expected for RO₂ from large VOCS.
960 However, the fraction of these RO₂ species is expected to be small for conditions of this campaign, even
961 if OH reactivity that is not explained by measured OH reactants is attributed to large VOCs. Therefore, it
962 seems unlikely that the mechanism suggested by Whalley et al. (2021) affects the observed discrepancies
963 in the radical budgets in this study.

964 It is interesting to point out that similar discrepancies in the OH and HO₂ budgets have been observed
965 during the HO_xComp campaign in July 2005 (Elshorbany et al., 2012). Although measurements were
966 only done for 3 days and despite that these were 14 years earlier than measurements in this work, the

967 chemical composition was similar with comparable values of NO_x, O₃, isoprene concentrations and of
968 OH reactivity. As observed in this study, a missing OH radical source in the range of 2 to 4 ppbv h⁻¹ was
969 needed to close the OH budget for low-NO chemical regimes. The lack of measured RO₂ radicals did not
970 allow to perform a measurement-only budget for HO₂ radicals. Nevertheless, model calculations
971 overestimated measured HO₂ radicals after the correction for RO₂ radical interferences (Fuchs et al., 2011)
972 by up to 30% at low NO (Elshorbany et al., 2012; Kanaya et al., 2012). Like in this study, good
973 agreement was found between modelled and measured OH and HO₂ radical concentrations only if an
974 unknown loss process for HO₂ radicals that would recycle OH was introduced.

975 **4.4 Potential role of the missing radical processes on the evaluation of the ozone production rate**

976 The good agreement of the odd oxygen production rates calculated by the two different methods (Section
977 3.1) not only gives high confidence in the measured peroxy radical concentrations but also confirms the
978 current chemical understanding of tropospheric ozone formation from the reaction of peroxy radicals with
979 NO. Therefore, results demonstrate that accurate predictions of radical concentrations in atmospheric
980 models are crucial to accurately predict the surface ozone level.

981 However, the significant level of the missing radical processes found in this study implies the difficulties
982 in the prediction of the radical concentrations by the models without constraining radicals by their
983 measurements. In low NO mixing ratios, there are two opposing effects of the missing radical processes
984 on the O₃ formation. At first, a missing OH source and therefore an underestimation of OH concentrations
985 by the models would lower the loss of NO₂ by the reduced reaction rate with OH, and essentially produce
986 more O₃ by its photolysis. Furthermore, the production of RO₂ would be under-predicted due to the lower
987 OH concentrations in the models. At the same time, an unexplained HO₂ sink would result in the over-
988 prediction in HO₂ concentrations and thus O₃ production. In high NO environments, missing RO₂ and
989 RO_x production processes would result in an underestimation of the O₃ production.

990

991 **5 Summary and conclusions**

992 Ambient measurements of atmospheric radicals, trace gases, and aerosol properties were performed
993 during the Jülich Atmospheric Chemistry Project campaign (JULIAC) using the atmospheric simulation
994 chamber SAPHIR at Forschungszentrum Jülich, Germany. Ambient air was continuously drawn at a high
995 rate into the chamber (1 hour residence time) through a 50 m high inlet line for one month in each season
996 throughout 2019.

997 For parts of the campaign, measurements of OH concentrations were achieved by two different methods,
998 laser-induced fluorescence with a chemical modulation system for zeroing (FZJ-LIF-CMR) and
999 differential optical absorption spectroscopy (FZJ-DOAS). Measurements of both instruments agreed
1000 within 11 % (Cho et al., 2021).

1001 The production rate of odd oxygen (O_x) was determined by using either measured HO₂ and RO₂
1002 concentrations or O₃ and NO₂ concentrations measured in the chamber and in the incoming flow. Results
1003 showed excellent agreement between the two different methods confirming that HO₂ and RO₂ are

1004 responsible for the formation of tropospheric O₃ and giving additional confidence in the reliability of
1005 peroxy radical concentration measurements performed in the JULIAC campaign.

1006 An analysis of the chemical budgets of OH, HO₂, RO₂ and RO_x radicals was performed for data obtained
1007 in the spring and summer periods of the campaign. On average, daytime radical turnover rates ranged
1008 between 3 to 6 ppbv h⁻¹ and 4 to 10 ppbv h⁻¹ in spring and summer, respectively, for OH, HO₂ and RO₂
1009 radicals, while total rates of RO_x initiation and termination reactions were below 2.0 ppbv h⁻¹. For most
1010 conditions, radical production and destruction rates highly depended on the turnover rate of the reaction
1011 of peroxy radicals with NO. For the total turnover rate of the sum of all radicals (RO_x), the photolysis of
1012 HONO and HCHO contributed most to the primary radical production and the reactions of OH with NO₂
1013 and RO₂ with HO₂ dominated the radical termination processes.

1014 Differences between radical production and destruction rates were often small and below the accuracy of
1015 the calculations in the JULIAC campaign in winter and autumn. However, for both spring and summer,
1016 an additional OH source is required to explain the observed discrepancy between production and
1017 destruction rates. The OH production rate of this source would need be on average 2 ppbv h⁻¹ and 3 ppbv
1018 h⁻¹ in the spring and summer period, respectively. This discrepancy is in the same range as observed for
1019 measurements at the same location during the HO_xComp campaign in July 2005 (Elshorbany et al., 2012).

1020 Discrepancies between production and destruction rates of OH radicals were highest for conditions with
1021 low NO mixing ratios in this study. This is similar to findings in other field campaigns in China (Tan et
1022 al., 2017; Tan et al., 2019; Whalley et al., 2021). The high reliability of radical data in this study gives
1023 further confidence that the discrepancies arise from unaccounted chemical processes rather than from
1024 instrumental artefacts.

1025 The highest unaccounted OH source with a rate of 3.0 ppbv h⁻¹ (51 % of the observed total OH
1026 destruction rate) is observed in the period from 5 August to 8 August (Case 1), when NO mixing ratios
1027 were less than 1 ppbv and median maximum temperature in the chamber were 31°C. At the same time, an
1028 additional HO₂ destruction process with a rate of up to 2.0 ppbv h⁻¹ is required to balance the HO₂
1029 production rate, while production and destruction rates for RO₂ radicals are well balanced. The opposing
1030 imbalances in the OH and HO₂ budgets could be due to an unknown mechanism that converts HO₂ to OH,
1031 or this could indicate a missing primary OH source and a similar fast, but independent termination
1032 reaction removing HO₂. If an unknown HO₂ to OH conversion mechanism played a major role, it would
1033 not explain the complete rate of the missing OH source. Since the missing OH source is slightly larger
1034 than the rate of the missing HO₂ sink, part of the missing OH source could have been originated from a
1035 missing primary OH production process, because also a small difference between the total RO_x
1036 production and destruction rates are observed. The missing RO_x source was up to 0.5 ppbv h⁻¹ for Case 1,
1037 but was even higher with a rate of 1.4 ppbv h⁻¹ in the summer, when temperature was highest (Case 2).
1038 Since the calculated reaction rate of the HO₂ and RO₂ radicals with NO were able to reproduce the
1039 observed O_x production within 1ppbv h⁻¹, the unknown missing processes do not seem to have a direct
1040 impact on net ozone production.

1041 For NO mixing ratios in range of 1 to 3 ppbv, production and destruction rates for OH and HO₂ radicals
1042 were balanced, while additional sources of RO₂ and RO_x having on average rates of 1.6 ppbv h⁻¹ and 0.4
1043 ppbv h⁻¹, respectively, were required to balance their production and destruction rates. Therefore, part of

1044 the missing RO₂ source can be explained by a primary radical source, but the remaining RO₂ source is
1045 still unresolved.

1046 For high NO mixing ratios above 3 ppbv, 4 to 5 ppbv h⁻¹, large discrepancies between production and
1047 destruction rates of HO₂ and RO₂ radicals were found, but the calculations for these conditions have a
1048 higher uncertainty due to low HO₂ and RO₂ concentrations close to background signals. Whereas the
1049 imbalance in the budget for HO₂ radicals is due to unaccounted loss processes, an additional RO₂
1050 production process is required to close the chemical budget for RO₂ radicals. For the same conditions, a
1051 primary RO_x source with a rate of 0.5 ppbv h⁻¹ was needed to balance the RO_x destruction rate. Therefore,
1052 the missing primary RO_x source is likely an unaccounted primary RO₂ source.

1053 Production of radicals from the oxidation of organic compounds by chlorine could have been one
1054 additional source. Unfortunately, the potential impact of chlorine chemistry could not be examined in the
1055 spring periods, when these conditions were experienced, because ClNO₂ measurements were not available.
1056 During times when ClNO₂ concentrations were measured, chlorine chemistry initiated by the photolysis
1057 of ClNO₂ did not significantly contribute to the radical production.

1058 For chemical conditions when the contribution of the reaction of HO₂ with NO to the OH production was
1059 reduced, i.e. at lower NO levels, other radical formation pathways such as isomerization reactions of RO₂
1060 radicals, OH formation from ozonolysis of alkenes or photolysis of multifunctional organic compounds
1061 could gain in importance and need to be properly accounted for. These processes remain relatively poorly
1062 constrained due to the lack of direct measurements of e.g., multifunctional organic compounds.

1063 Although the exact mechanism for the missing production or destruction processes for OH, HO₂ and RO₂
1064 radicals could not be determined from measurements in this campaign, knowing the magnitudes of the
1065 missing radical processes gives indicative information about the disagreements of model simulations and
1066 observations for radicals and secondary air pollutants.

1067 More investigations of the chemical budgets of radicals for example in environments with high NO
1068 mixing ratios including the determination of the impact of chlorine chemistry and with a detailed
1069 characterization of the chemical composition of air masses with respect to the presence of complex
1070 organic compounds would be beneficial for the understanding of radical chemistry as well as of the
1071 formation of secondary air pollution such as ozone.

1072

1073 **Code and data availability**

1074 Data of the JULIAC campaign analyzed in this work is available from the Jülich Data repository
1075 (<https://doi.org/10.26165/JUELICH-DATA/3J80BW>, Cho et al., 2022).

1076

1077 **Author contributions**

1078 AH designed JULIAC campaign and organized it together with HF and FH. CC performed the
1079 measurements of radicals, analyzed the data, and wrote the paper together with AN and HF. All co-
1080 authors contributed with data and helped the writing by intensive discussions of the manuscript.

1081

1082 **Competing interests**

1083 The authors declare that they have no conflict of interest.

1084

1085 **Financial Support**

1086 This project has received funding from the European Research Council (ERC) under the European
1087 Union's Horizon 2020 research and innovation program (SARLEP grant agreement no. 681529) and from
1088 the European Commission (EC) (Eurochamp 2020 project, grant agreement no. 730997).

1089

1090 **References**

1091 Atkinson, R., Baulch, D. L., Cox, R. A., Crowley, J. N., Hampson, R. F., Hynes, R. G., Jenkin, M. E.,
1092 Rossi, M. J., and Troe, J.: Evaluated kinetic and photochemical data for atmospheric chemistry: Volume I
1093 - gas phase reactions of O_x, HO_x, NO_x and SO_x species, *Atmos. Chem. Phys.*, 4, 1461-1738,
1094 doi:10.5194/acp-4-1461-2004, 2004.

1095

1096 Atkinson, R., Baulch, D. L., Cox, R. A., Crowley, J. N., Hampson, R. F., Hynes, R. G., Jenkin, M. E.,
1097 Rossi, M. J., Troe, J., and Subcommittee, I.: Evaluated kinetic and photochemical data for atmospheric
1098 chemistry: Volume II - gas phase reactions of organic species, *Atmos. Chem. Phys.*, 6, 3625-4055,
1099 doi:10.5194/acp-6-3625-2006, 2006.

1100

1101 Bloss, W. J., Lee, J. D., Johnson, G. P., Sommariva, R., Heard, D. E., Saiz-Lopez, A., Plane, J. M. C.,
1102 McFiggans, G., Coe, H., Flynn, M., Williams, P., Rickard, A. R., and Fleming, Z. L.: Impact of halogen
1103 monoxide chemistry upon boundary layer OH and HO₂ concentrations at a coastal site, *Geophysical*
1104 *Research Letters*, 32, doi:10.1029/2004GL022084, 2005.

1105

1106 BMEL: (Federal Ministry of Food and Agriculture) : Ergebnisse der Waldzustandserhebung 2020, in,
1107 Bonn, Germany, 2021.

1108

1109 Bohn, B., Rohrer, F., Brauers, T., and Wahner, A.: Actinometric measurements of NO₂ photolysis
1110 frequencies in the atmosphere simulation chamber SAPHIR, *Atmos. Chem. Phys.*, 5, 493-503,
1111 doi:10.5194/acp-5-493-2005, 2005.

1112

1113 Bohn, B., and Zilken, H.: Model-aided radiometric determination of photolysis frequencies in a sunlit
1114 atmosphere simulation chamber, *Atmos. Chem. Phys.*, 5, 191-206, doi:10.5194/acp-5-191-2005, 2005.

1115

1116 Brune, W. H., Baier, B. C., Thomas, J., Ren, X., Cohen, R. C., Pusede, S. E., Browne, E. C., Goldstein, A.
1117 H., Gentner, D. R., Keutsch, F. N., Thornton, J. A., Harrold, S., Lopez-Hilfiker, F. D., and Wennberg, P.

1118 O.: Ozone production chemistry in the presence of urban plumes, *Faraday Discuss.*, 189, 169-189,
1119 doi:10.1039/C5FD00204D, 2016.

1120

1121 Cazorla, M., Brune, W. H., Ren, X., and Lefer, B.: Direct measurement of ozone production rates in
1122 Houston in 2009 and comparison with two estimation methods, *Atmos. Chem. Phys.*, 12, 1203-1212,
1123 doi:10.5194/acp-12-1203-2012, 2012.

1124

1125 Chen, S., Ren, X., Mao, J., Chen, Z., Brune, W. H., Lefer, B., Rappenglück, B., Flynn, J., Olson, J., and
1126 Crawford, J. H.: A comparison of chemical mechanisms based on TRAMP-2006 field data, *Atmos.*
1127 *Environ.*, 44, 4116-4125, doi:10.1016/j.atmosenv.2009.05.027, 2010.

1128

1129 Cho, C., Hofzumahaus, A., Fuchs, H., Dorn, H. P., Glowania, M., Holland, F., Rohrer, F., Vardhan, V.,
1130 Kiendler-Scharr, A., Wahner, A., and Novelli, A.: Characterization of a chemical modulation reactor
1131 (CMR) for the measurement of atmospheric concentrations of hydroxyl radicals with a laser-induced
1132 fluorescence instrument, *Atmos. Meas. Tech.*, 14, 1851-1877, doi:10.5194/amt-14-1851-2021, 2021.

1133

1134 Cox, R. A., Ammann, M., Crowley, J. N., Herrmann, H., Jenkin, M. E., McNeill, V. F., Mellouki, A.,
1135 Troe, J., and Wallington, T. J.: Evaluated kinetic and photochemical data for atmospheric chemistry:
1136 Volume VII – Criegee intermediates, *Atmos. Chem. Phys.*, 20, 13497-13519, doi:10.5194/acp-20-13497-
1137 2020, 2020.

1138

1139 Crouse, J. D., Paulot, F., Kjaergaard, H. G., and Wennberg, P. O.: Peroxy radical isomerization in the
1140 oxidation of isoprene, *Phys. Chem. Chem. Phys.*, 13, 13607-13613, doi:10.1039/C1CP21330J, 2011.

1141

1142 Crouse, J. D., Knap, H. C., Ørnsø, K. B., Jørgensen, S., Paulot, F., Kjaergaard, H. G., and Wennberg, P.
1143 O.: Atmospheric Fate of Methacrolein. 1. Peroxy Radical Isomerization Following Addition of OH and
1144 O₂, *J. Phys. Chem. A*, 116, 5756-5762, doi:10.1021/jp211560u, 2012.

1145

1146 da Silva, G., Graham, C., and Wang, Z.-F.: Unimolecular β-hydroxyperoxy radical decomposition with
1147 OH recycling in the photochemical oxidation of isoprene, *Environ. Sci. Technol.*, 44, 250-256,
1148 doi:10.1021/es900924d, 2010.

1149

1150 Dillon, T. J., and Crowley, J. N.: Direct detection of OH formation in the reactions of HO₂ with
1151 CH₃C(O)O₂ and other substituted peroxy radicals, *Atmos. Chem. Phys.*, 8, 4877-4889, doi:10.5194/acp-8-
1152 4877-2008, 2008.

1153

1154 Dusanter, S., Vimal, D., Stevens, P. S., Volkamer, R., Molina, L. T., Baker, A., Meinardi, S., Blake, D.,
1155 Sheehy, P., Merten, A., Zhang, R., Zheng, J., Fortner, E. C., Junkermann, W., Dubey, M., Rahn, T.,
1156 Eichinger, B., Lewandowski, P., Prueger, J., and Holder, H.: Measurements of OH and HO₂
1157 concentrations during the MCMA-2006 field campaign – Part 2: Model comparison and radical budget,
1158 *Atmos. Chem. Phys.*, 9, 6655-6675, doi:10.5194/acp-9-6655-2009, 2009.

1159

1160 Ehhalt, D. H., and Rohrer, F.: Dependence of the OH concentration on solar UV, *J. Geophys. Res.:*
1161 *Atmos.*, 105, 3565-3571, doi:10.1029/1999jd901070, 2000.

1162

1163 Elshorbany, Y. F., Kleffmann, J., Hofzumahaus, A., Kurtenbach, R., Wiesen, P., Brauers, T., Bohn, B.,
1164 Dorn, H.-P., Fuchs, H., Holland, F., Rohrer, F., Tillmann, R., Wegener, R., Wahner, A., Kanaya, Y.,
1165 Yoshino, A., Nishida, S., Kajii, Y., Martinez, M., Kubistin, D., Harder, H., Lelieveld, J., Elste, T., Plass-
1166 Dülmer, C., Stange, G., Berresheim, H., and Schurath, U.: HOx budgets during HOxComp: A case study
1167 of HOx chemistry under NOx-limited conditions, *J. Geophys. Res.: Atmos.*, 117,
1168 doi:10.1029/2011JD017008, 2012.

1169

1170 Fan, S., and Li, Y.: The impacts of marine-emitted halogens on OH radicals in East Asia during summer,
1171 *Atmos. Chem. Phys.*, 22, 7331-7351, doi:10.5194/acp-22-7331-2022, 2022.

1172

1173 Fishman, J., and Carney, T. A.: A one-dimensional photochemical model of the troposphere with
1174 planetary boundary-layer parameterization, *J. Atmos. Chem.*, 1, 351-376, doi:10.1007/BF00053800, 1984.
1175

1176

1177 Fuchs, H., Holland, F., and Hofzumahaus, A.: Measurement of tropospheric RO₂ and HO₂ radicals by a
1178 laser-induced fluorescence instrument, *Rev. Sci. Instrum.*, 79, 084104, doi:10.1063/1.2968712, 2008.

1179

1180 Fuchs, H., Bohn, B., Hofzumahaus, A., Holland, F., Lu, K. D., Nehr, S., Rohrer, F., and Wahner, A.:
1181 Detection of HO₂ by laser-induced fluorescence: calibration and interferences from RO₂ radicals, *Atmos.*
1182 *Meas. Tech.*, 4, 1209-1225, doi:10.5194/amt-4-1209-2011, 2011.

1183

1184 Fuchs, H., Dorn, H. P., Bachner, M., Bohn, B., Brauers, T., Gomm, S., Hofzumahaus, A., Holland, F.,
1185 Nehr, S., Rohrer, F., Tillmann, R., and Wahner, A.: Comparison of OH concentration measurements by
1186 DOAS and LIF during SAPHIR chamber experiments at high OH reactivity and low NO concentration,
1187 *Atmos. Meas. Tech.*, 5, 1611-1626, doi:10.5194/amt-5-1611-2012, 2012.

1188

1189 Fuchs, H., Hofzumahaus, A., Rohrer, F., Bohn, B., Brauers, T., Dorn, H. P., Häsel, R., Holland, F.,
1190 Kaminski, M., Li, X., Lu, K., Nehr, S., Tillmann, R., Wegener, R., and Wahner, A.: Experimental
1191 evidence for efficient hydroxyl radical regeneration in isoprene oxidation, *Nat. Geosci.*, 6, 1023-1026,
1192 doi:10.1038/ngeo1964, 2013.

1193

1194 Fuchs, H., Acir, I. H., Bohn, B., Brauers, T., Dorn, H. P., Häsel, R., Hofzumahaus, A., Holland, F.,
1195 Kaminski, M., Li, X., Lu, K., Lutz, A., Nehr, S., Rohrer, F., Tillmann, R., Wegener, R., and Wahner, A.:
1196 OH regeneration from methacrolein oxidation investigated in the atmosphere simulation chamber
1197 SAPHIR, *Atmos. Chem. Phys.*, 14, 7895-7908, doi:10.5194/acp-14-7895-2014, 2014.

1198

1199 Fuchs, H., Novelli, A., Rolletter, M., Hofzumahaus, A., Pfannerstill, E. Y., Kessel, S., Edtbauer, A.,
1200 Williams, J., Michoud, V., Dusanter, S., Locoge, N., Zannoni, N., Gros, V., Truong, F., Sarda-Esteve, R.,
1201 Cryer, D. R., Brumby, C. A., Whalley, L. K., Stone, D., Seakins, P. W., Heard, D. E., Schoemaeker, C.,
1202 Blocquet, M., Coudert, S., Batut, S., Fittschen, C., Thames, A. B., Brune, W. H., Ernest, C., Harder, H.,
1203 Muller, J. B. A., Elste, T., Kubistin, D., Andres, S., Bohn, B., Hohaus, T., Holland, F., Li, X., Rohrer, F.,

- 1204 Kiendler-Scharr, A., Tillmann, R., Wegener, R., Yu, Z., Zou, Q., and Wahner, A.: Comparison of OH
1205 reactivity measurements in the atmospheric simulation chamber SAPHIR, *Atmos. Meas. Tech.*, 10, 4023-
1206 4053, doi:10.5194/amt-10-4023-2017, 2017.
- 1207
1208 Fuchs, H., Albrecht, S., Acir, I., Bohn, B., Breitenlechner, M., Dorn, H. P., Gkatzelis, G. I., Hofzumahaus,
1209 A., Holland, F., Kaminski, M., Keutsch, F. N., Novelli, A., Reimer, D., Rohrer, F., Tillmann, R.,
1210 Vereecken, L., Wegener, R., Zaytsev, A., Kiendler-Scharr, A., and Wahner, A.: Investigation of the
1211 oxidation of methyl vinyl ketone (MVK) by OH radicals in the atmospheric simulation chamber SAPHIR,
1212 *Atmos. Chem. Phys.*, 18, 8001-8016, doi:10.5194/acp-18-8001-2018, 2018.
- 1213
1214 George, I. J., Vlasenko, A., Slowik, J. G., Broekhuizen, K., and Abbatt, J. P. D.: Heterogeneous oxidation
1215 of saturated organic aerosols by hydroxyl radicals: uptake kinetics, condensed-phase products, and
1216 particle size change, *Atmos. Chem. Phys.*, 7, 4187-4201, doi:10.5194/acp-7-4187-2007, 2007.
- 1217
1218 George, I. J., Matthews, P. S. J., Whalley, L. K., Brooks, B., Goddard, A., Baeza-Romero, M. T., and
1219 Heard, D. E.: Measurements of uptake coefficients for heterogeneous loss of HO₂ onto submicron
1220 inorganic salt aerosols, *Phys. Chem. Chem. Phys.*, 15, 12829-12845, doi:10.1039/C3CP51831K, 2013.
- 1221
1222 Glowania, M., Rohrer, F., Dorn, H. P., Hofzumahaus, A., Holland, F., Kiendler-Scharr, A., Wahner, A.,
1223 and Fuchs, H.: Comparison of formaldehyde measurements by Hantzsch, CRDS and DOAS in the
1224 SAPHIR chamber, *Atmos. Meas. Tech. Discuss.*, 2021, 1-23, doi:10.5194/amt-2021-10, 2021.
- 1225
1226 Goldberg, D. L., Vinciguerra, T. P., Hosley, K. M., Loughner, C. P., Canty, T. P., Salawitch, R. J., and
1227 Dickerson, R. R.: Evidence for an increase in the ozone photochemical lifetime in the eastern United
1228 States using a regional air quality model, *J. Geophys. Res.: Atmos.*, 120, 12778-12793,
1229 doi:10.1002/2015JD023930, 2015.
- 1230
1231 Goldstein, A. H., Fan, S. M., Goulden, M. L., Munger, J. W., and Wofsy, S. C.: Emissions of ethene,
1232 propene, and 1-butene by a midlatitude forest, *Journal of Geophysical Research: Atmospheres*, 101, 9149-
1233 9157, doi:10.1029/96JD00334, 1996.
- 1234
1235 Goldstein, A. H., and Galbally, I. E.: Known and Unexplored Organic Constituents in the Earth's
1236 Atmosphere, *Environ. Sci. Technol.*, 41, 1514-1521, doi:10.1021/es072476p, 2007.
- 1237
1238 Griffith, S. M., Hansen, R. F., Dusanter, S., Stevens, P. S., Alaghmand, M., Bertman, S. B., Carroll, M. A.,
1239 Erickson, M., Galloway, M., Grossberg, N., Hottle, J., Hou, J., Jobson, B. T., Kamrath, A., Keutsch, F.
1240 N., Lefer, B. L., Mielke, L. H., O'Brien, A., Shepson, P. B., Thurlow, M., Wallace, W., Zhang, N., and
1241 Zhou, X. L.: OH and HO₂ radical chemistry during PROPHET 2008 and CABINEX 2009 - Part 1:
1242 Measurements and model comparison, *Atmos. Chem. Phys.*, 13, 5403-5423, doi:10.5194/acp-13-5403-
1243 2013, 2013.
- 1244
1245 Griffith, S. M., Hansen, R. F., Dusanter, S., Michoud, V., Gilman, J. B., Kuster, W. C., Veres, P. R.,
1246 Graus, M., de Gouw, J. A., Roberts, J., Young, C., Washenfelder, R., Brown, S. S., Thalman, R.,
1247 Waxman, E., Volkamer, R., Tsai, C., Stutz, J., Flynn, J. H., Grossberg, N., Lefer, B., Alvarez, S. L.,

- 1248 Rappenglueck, B., Mielke, L. H., Osthoff, H. D., and Stevens, P. S.: Measurements of hydroxyl and
1249 hydroperoxy radicals during CalNex-LA: Model comparisons and radical budgets, *J. Geophys. Res.:*
1250 *Atmos.*, 121, 4211-4232, doi:10.1002/2015jd024358, 2016.
- 1251
1252 Groß, C. B. M., Dillon, T. J., Schuster, G., Lelieveld, J., and Crowley, J. N.: Direct Kinetic Study of OH
1253 and O₃ Formation in the Reaction of CH₃C(O)O₂ with HO₂, *J. Phys. Chem. A*, 118, 974-985,
1254 doi:10.1021/jp412380z, 2014.
- 1255
1256 Häsel, R., Brauers, T., Holland, F., and Wahner, A.: Development and application of a new mobile
1257 LOPAP instrument for the measurement of HONO altitude profiles in the planetary boundary layer,
1258 *Atmos. Meas. Tech. Discuss.*, 2009, 2027-2054, doi:10.5194/amtd-2-2027-2009, 2009.
- 1259
1260 Han, S., Bian, H., Feng, Y., Liu, A., Li, X., Zeng, F., and Zhang, X.: Analysis of the Relationship
1261 between O₃, NO and NO₂ in Tianjin, China, *Aerosol Air Qual. Res.*, 11, 128-139,
1262 doi:10.4209/aaqr.2010.07.0055, 2011.
- 1263
1264 Handisides, G. M., Plass-Dülmer, C., Gilge, S., Bingemer, H., and Berresheim, H.: Hohenpeissenberg
1265 Photochemical Experiment (HOPE 2000): Measurements and photostationary state calculations of OH
1266 and peroxy radicals, *Atmos. Chem. Phys.*, 3, 1565-1588, doi:10.5194/acp-3-1565-2003, 2003.
- 1267
1268 Hasson, A. S., Tyndall, G. S., and Orlando, J. J.: A Product Yield Study of the Reaction of HO₂ Radicals
1269 with Ethyl Peroxy (C₂H₅O₂), Acetyl Peroxy (CH₃C(O)O₂), and Acetonyl Peroxy (CH₃C(O)CH₂O₂)
1270 Radicals, *J. Phys. Chem. A*, 108, 5979-5989, doi:10.1021/jp048873t, 2004.
- 1271
1272 Hens, K., Novelli, A., Martinez, M., Auld, J., Axinte, R., Bohn, B., Fischer, H., Keronen, P., Kubistin, D.,
1273 Nölscher, A. C., Oswald, R., Paasonen, P., Petäjä, T., Regelin, E., Sander, R., Sinha, V., Sipilä, M.,
1274 Taraborrelli, D., Tatum Ernest, C., Williams, J., Lelieveld, J., and Harder, H.: Observation and modelling
1275 of HOx radicals in a boreal forest, *Atmos. Chem. Phys.*, 14, 8723-8747, doi:10.5194/acp-14-8723-2014,
1276 2014.
- 1277
1278 Hofzumahaus, A., Rohrer, F., Lu, K., Bohn, B., Brauers, T., Chang, C.-C., Fuchs, H., Holland, F., Kita,
1279 K., Kondo, Y., Li, X., Lou, S., Shao, M., Zeng, L., Wahner, A., and Zhang, Y.: Amplified trace gas
1280 removal in the troposphere, *Science*, 324, 1702-1704, doi:10.1126/science.1164566, 2009.
- 1281
1282 Hofzumahaus, A., and Heard, D. H.: Assessment of local HOx and ROx measurement techniques:
1283 achievements, challenges, and future directions - Outcomes of the 2015 international HOx workshop,
1284 Forschungszentrum Jülich, Jülich, 20-21, 2016.
- 1285
1286 Holland, F., Hofzumahaus, A., Schäfer, J., Kraus, A., and Pätz, H.-W.: Measurements of OH and HO₂
1287 radical concentrations and photolysis frequencies during BERLIOZ, *J. Geophys. Res.: Atmos.*, 108, 8246,
1288 doi:10.1029/2001jd001393, 2003.
- 1289

1290 J. B. Burkholder, S. P. S., J. Abbatt, J. R. Barker, C. Cappa, J. D. Crouse, T. S. Dibble, R. E. Huie, C. E.
1291 Kolb, M. J. Kurylo, V. L. Orkin, C. J. Percival, D. M. Wilmouth, and P. H. Wine: Chemical Kinetics and
1292 Photochemical Data for Use in Atmospheric Studies, Evaluation No. 19, Jet Propulsion Laboratory,
1293 Pasadena, 2019.

1294
1295 Jenkin, M. E., Valorso, R., Aumont, B., and Rickard, A. R.: Estimation of rate coefficients and branching
1296 ratios for reactions of organic peroxy radicals for use in automated mechanism construction, *Atmos.*
1297 *Chem. Phys.*, 19, 7691-7717, doi:10.5194/acp-19-7691-2019, 2019.

1298
1299 Jordan, A., Haidacher, S., Hanel, G., Hartungen, E., Märk, L., Seehauser, H., Schottkowsky, R., Sulzer, P.,
1300 and Märk, T. D.: A high resolution and high sensitivity proton-transfer-reaction time-of-flight mass
1301 spectrometer (PTR-TOF-MS), *Int. J. Mass Spectrom.*, 286, 122-128, doi:10.1016/j.ijms.2009.07.005,
1302 2009.

1303
1304 Kaminski, M., Fuchs, H., Acir, I. H., Bohn, B., Brauers, T., Dorn, H. P., Häsel, R., Hofzumahaus, A., Li,
1305 X., Lutz, A., Nehr, S., Rohrer, F., Tillmann, R., Vereecken, L., Wegener, R., and Wahner, A.:
1306 Investigation of the β -pinene photooxidation by OH in the atmosphere simulation chamber SAPHIR,
1307 *Atmos. Chem. Phys.*, 17, 6631-6650, doi:10.5194/acp-17-6631-2017, 2017.

1308
1309 Kanaya, Y., Cao, R., Akimoto, H., Fukuda, M., Komazaki, Y., Yokouchi, Y., Koike, M., Tanimoto, H.,
1310 Takegawa, N., and Kondo, Y.: Urban photochemistry in central Tokyo: 1. Observed and modeled OH and
1311 HO₂ radical concentrations during the winter and summer of 2004, *J. Geophys. Res.: Atmos.*, 112,
1312 doi:10.1029/2007jd008670, 2007.

1313
1314 Kanaya, Y., Hofzumahaus, A., Dorn, H. P., Brauers, T., Fuchs, H., Holland, F., Rohrer, F., Bohn, B.,
1315 Tillmann, R., Wegener, R., Wahner, A., Kajii, Y., Miyamoto, K., Nishida, S., Watanabe, K., Yoshino, A.,
1316 Kubistin, D., Martinez, M., Rudolf, M., Harder, H., Berresheim, H., Elste, T., Plass-Dülmer, C., Stange,
1317 G., Kleffmann, J., Elshorbany, Y., and Schurath, U.: Comparisons of observed and modeled OH and HO₂
1318 concentrations during the ambient measurement period of the HO_xComp field campaign, *Atmos. Chem.*
1319 *Phys.*, 12, 2567-2585, doi:10.5194/acp-12-2567-2012, 2012.

1320
1321 Kim, S., Wolfe, G. M., Mauldin, L., Cantrell, C., Guenther, A., Karl, T., Turnipseed, A., Greenberg, J.,
1322 Hall, S. R., Ullmann, K., Apel, E., Hornbrook, R., Kajii, Y., Nakashima, Y., Keutsch, F. N., DiGangi, J.
1323 P., Henry, S. B., Kaser, L., Schnitzhofer, R., Graus, M., Hansel, A., Zheng, W., and Flocke, F. F.:
1324 Evaluation of HO_x sources and cycling using measurement-constrained model calculations in a 2-methyl-
1325 3-butene-2-ol (MBO) and monoterpene (MT) dominated ecosystem, *Atmos. Chem. Phys.*, 13, 2031-2044,
1326 doi:10.5194/acp-13-2031-2013, 2013.

1327
1328 Kleffmann, J., Lörzer, J. C., Wiesen, P., Kern, C., Trick, S., Volkamer, R., Rodenas, M., and Wirtz, K.:
1329 Intercomparison of the DOAS and LOPAP techniques for the detection of nitrous acid (HONO), *Atmos.*
1330 *Environ.*, 40, 3640-3652, doi:10.1016/j.atmosenv.2006.03.027, 2006.

1331

1332 Kleinman, L. I., Daum, P. H., Lee, Y.-N., Nunnermacker, L. J., Springston, S. R., Weinstein-Lloyd, J.,
1333 and Rudolph, J.: Ozone production efficiency in an urban area, *J. Geophys. Res.: Atmos.*, 107, ACH 23-
1334 21-ACH 23-12, doi:10.1029/2002JD002529, 2002.

1335
1336 Komenda, M., Schaub, A., and Koppmann, R.: Description and characterization of an on-line system for
1337 long-term measurements of isoprene, methyl vinyl ketone, and methacrolein in ambient air, *J.*
1338 *Chromatogr. A*, 995, 185-201, doi:10.1016/S0021-9673(03)00518-1, 2003.

1339
1340 Konrad, S., Schmitz, T., Buers, H.-J., Houben, N., Mannschreck, K., Mihelcic, D., Müsgen, P., Pätz, H.-
1341 W., Holland, F., Hofzumahaus, A., Schäfer, H.-J., Schröder, S., Volz-Thomas, A., Bächmann, K.,
1342 Schlomski, S., Moortgat, G., and Großmann, D.: Hydrocarbon measurements at Pabstthum during the
1343 BERLIOZ campaign and modeling of free radicals, *J. Geophys. Res.: Atmos.*, 108,
1344 doi:10.1029/2001JD000866, 2003.

1345
1346 Kubistin, D., Harder, H., Martinez, M., Rudolf, M., Sander, R., Bozem, H., Eerdeken, G., Fischer, H.,
1347 Gurk, C., Klüpfel, T., Königstedt, R., Parchatka, U., Schiller, C. L., Stickler, A., Taraborrelli, D.,
1348 Williams, J., and Lelieveld, J.: Hydroxyl radicals in the tropical troposphere over the Suriname rainforest:
1349 comparison of measurements with the box model MECCA, *Atmos. Chem. Phys.*, 10, 9705-9728,
1350 doi:10.5194/acp-10-9705-2010, 2010.

1351
1352 Lakey, P. S. J., George, I. J., Whalley, L. K., Baeza-Romero, M. T., and Heard, D. E.: Measurements of
1353 the HO₂ Uptake Coefficients onto Single Component Organic Aerosols, *Environ. Sci. Technol.*, 49, 4878-
1354 4885, doi:10.1021/acs.est.5b00948, 2015.

1355
1356 Lelieveld, J., Butler, T. M., Crowley, J. N., Dillon, T. J., Fischer, H., Ganzeveld, L., Harder, H., Lawrence,
1357 M. G., Martinez, M., Taraborrelli, D., and Williams, J.: Atmospheric oxidation capacity sustained by a
1358 tropical forest, *Nature*, 452, 737, doi:10.1038/nature06870, 2008.

1359
1360 Lou, S., Holland, F., Rohrer, F., Lu, K., Bohn, B., Brauers, T., Chang, C. C., Fuchs, H., Häseler, R., Kita,
1361 K., Kondo, Y., Li, X., Shao, M., Zeng, L., Wahner, A., Zhang, Y., Wang, W., and Hofzumahaus, A.:
1362 Atmospheric OH reactivities in the Pearl River Delta – China in summer 2006: measurement and model
1363 results, *Atmos. Chem. Phys.*, 10, 11243-11260, doi:10.5194/acp-10-11243-2010, 2010.

1364
1365 Lu, K. D., Hofzumahaus, A., Holland, F., Bohn, B., Brauers, T., Fuchs, H., Hu, M., Häseler, R., Kita, K.,
1366 Kondo, Y., Li, X., Lou, S. R., Oebel, A., Shao, M., Zeng, L. M., Wahner, A., Zhu, T., Zhang, Y. H., and
1367 Rohrer, F.: Missing OH source in a suburban environment near Beijing: observed and modelled OH and
1368 HO₂ concentrations in summer 2006, *Atmos. Chem. Phys.*, 13, 1057-1080, doi:10.5194/acp-13-1057-
1369 2013, 2013.

1370
1371 Lu, K. D., Rohrer, F., Holland, F., Fuchs, H., Brauers, T., Oebel, A., Dlugi, R., Hu, M., Li, X., Lou, S. R.,
1372 Shao, M., Zhu, T., Wahner, A., Zhang, Y. H., and Hofzumahaus, A.: Nighttime observation and
1373 chemistry of HO_x in the Pearl River Delta and Beijing in summer 2006, *Atmos. Chem. Phys.*, 14, 4979-
1374 4999, doi:10.5194/acp-14-4979-2014, 2014.

1375

1376 Ma, X., Tan, Z., Lu, K., Yang, X., Liu, Y., Li, S., Li, X., Chen, S., Novelli, A., Cho, C., Zeng, L., Wahner,
1377 A., and Zhang, Y.: Winter photochemistry in Beijing: Observation and model simulation of OH and HO₂
1378 radicals at an urban site, *Sci. Tot. Environ.*, 685, 85-95, doi:10.1016/j.scitotenv.2019.05.329, 2019.

1379
1380 Malkin, T. L., Goddard, A., Heard, D. E., and Seakins, P. W.: Measurements of OH and HO₂ yields from
1381 the gas phase ozonolysis of isoprene, *Atmos. Chem. Phys.*, 10, 1441-1459, doi:10.5194/acp-10-1441-
1382 2010, 2010.

1383
1384 Mao, J., Ren, X., Chen, S., Brune, W. H., Chen, Z., Martinez, M., Harder, H., Lefer, B., Rappenglück, B.,
1385 Flynn, J., and Leuchner, M.: Atmospheric oxidation capacity in the summer of Houston 2006:
1386 Comparison with summer measurements in other metropolitan studies, *Atmos. Environ.*, 44, 4107-4115,
1387 doi:doi.org/10.1016/j.atmosenv.2009.01.013, 2010.

1388
1389 Mao, J., Ren, X., Zhang, L., Van Duin, D. M., Cohen, R. C., Park, J. H., Goldstein, A. H., Paulot, F.,
1390 Beaver, M. R., Crounse, J. D., Wennberg, P. O., DiGangi, J. P., Henry, S. B., Keutsch, F. N., Park, C.,
1391 Schade, G. W., Wolfe, G. M., Thornton, J. A., and Brune, W. H.: Insights into hydroxyl measurements
1392 and atmospheric oxidation in a California forest, *Atmos. Chem. Phys.*, 12, 8009-8020, doi:10.5194/acp-
1393 12-8009-2012, 2012.

1394
1395 Martinez, M., Harder, H., Kovacs, T. A., Simpas, J. B., Bassis, J., Leshner, R., Brune, W. H., Frost, G. J.,
1396 Williams, E. J., Stroud, C. A., Jobson, B. T., Roberts, J. M., Hall, S. R., Shetter, R. E., Wert, B., Fried, A.,
1397 Alicke, B., Stutz, J., Young, V. L., White, A. B., and Zamora, R. J.: OH and HO₂ concentrations, sources,
1398 and loss rates during the Southern Oxidants Study in Nashville, Tennessee, summer 1999, *J. Geophys.*
1399 *Res.: Atmos.*, 108, doi:10.1029/2003JD003551, 2003.

1400
1401 Mihelcic, D., Holland, F., Hofzumahaus, A., Hoppe, L., Konrad, S., Müsgen, P., Pätz, H.-W., Schäfer, H.-
1402 J., Schmitz, T., Volz-Thomas, A., Bächmann, K., Schlomski, S., Platt, U., Geyer, A., Alicke, B., and
1403 Moortgat, G. K.: Peroxy radicals during BERLIOZ at Pabstthum: Measurements, radical budgets and
1404 ozone production, *J. Geophys. Res.: Atmos.*, 108, doi:10.1029/2001JD001014, 2003.

1405
1406 Nehr, S., Bohn, B., Fuchs, H., Hofzumahaus, A., and Wahner, A.: HO₂ formation from the OH + benzene
1407 reaction in the presence of O₂, *Physical Chemistry Chemical Physics*, 13, 10699-10708,
1408 doi:10.1039/C1CP20334G, 2011.

1409
1410 Nehr, S., Bohn, B., Dorn, H. P., Fuchs, H., Häsel, R., Hofzumahaus, A., Li, X., Rohrer, F., Tillmann, R.,
1411 and Wahner, A.: Atmospheric photochemistry of aromatic hydrocarbons: OH budgets during SAPHIR
1412 chamber experiments, *Atmos. Chem. Phys.*, 14, 6941-6952, doi:10.5194/acp-14-6941-2014, 2014.

1413
1414 Niether, D., Cho, C., Rohrer, F. H., A. Novelli, A., Holland, F., Fuchs, H., Wesolek, C., Bohn, B., and
1415 Wahner, A. K.-S., A. Tillmann, R.: Seasonal ozone production rate measurements by use of SAPHIR as a
1416 large continuous flow reactor during the JULIAC campaign, *Atmos. Chem. Phys.*, In preparation, 2022.

1417
1418 Novelli, A., Hens, K., Tatum Ernest, C., Kubistin, D., Regelin, E., Elste, T., Plass-Dülmer, C., Martinez,
1419 M., Lelieveld, J., and Harder, H.: Characterisation of an inlet pre-injector laser-induced fluorescence

1420 instrument for the measurement of atmospheric hydroxyl radicals, *Atmos. Meas. Tech.*, 7, 3413-3430,
1421 doi:10.5194/amt-7-3413-2014, 2014.

1422

1423 Novelli, A., Kaminski, M., Rolletter, M., Acir, I. H., Bohn, B., Dorn, H. P., Li, X., Lutz, A., Nehr, S.,
1424 Rohrer, F., Tillmann, R., Wegener, R., Holland, F., Hofzumahaus, A., Kiendler-Scharr, A., Wahner, A.,
1425 and Fuchs, H.: Evaluation of OH and HO₂ concentrations and their budgets during photooxidation of 2-
1426 methyl-3-butene-2-ol (MBO) in the atmospheric simulation chamber SAPHIR, *Atmos. Chem. Phys.*, 18,
1427 11409-11422, doi:10.5194/acp-18-11409-2018, 2018.

1428

1429 Novelli, A., Vereecken, L., Bohn, B., Dorn, H. P., Gkatzelis, G. I., Hofzumahaus, A., Holland, F., Reimer,
1430 D., Rohrer, F., Rosanka, S., Taraborrelli, D., Tillmann, R., Wegener, R., Yu, Z., Kiendler-Scharr, A.,
1431 Wahner, A., and Fuchs, H.: Importance of isomerization reactions for OH radical regeneration from the
1432 photo-oxidation of isoprene investigated in the atmospheric simulation chamber SAPHIR, *Atmos. Chem.*
1433 *Phys.*, 20, 3333-3355, doi:10.5194/acp-20-3333-2020, 2020.

1434

1435 Novelli, A., Cho, C., Fuchs, H., Hofzumahaus, A., Rohrer, F., Tillmann, R., Kiendler-Scharr, A., Wahner,
1436 A., and Vereecken, L.: Experimental and theoretical study on the impact of a nitrate group on the
1437 chemistry of alkoxy radicals, *Phys. Chem. Chem. Phys.*, 23, 5474-5495, doi:10.1039/d0cp05555g, 2021.

1438

1439 Osthoff, H. D., Roberts, J. M., Ravishankara, A. R., Williams, E. J., Lerner, B. M., Sommariva, R., Bates,
1440 T. S., Coffman, D., Quinn, P. K., Dibb, J. E., Stark, H., Burkholder, J. B., Talukdar, R. K., Meagher, J.,
1441 Fehsenfeld, F. C., and Brown, S. S.: High levels of nitryl chloride in the polluted subtropical marine
1442 boundary layer, *Nature Geoscience*, 1, 324-328, doi:10.1038/ngeo177, 2008.

1443

1444 Peeters, J., Nguyen, T., and Vereecken, L.: HO_x radical regeneration in the oxidation of isoprene, *Phys.*
1445 *Chem. Chem. Phys.*, 11, 5935-5939, doi:10.1039/b908511d, 2009.

1446

1447 Peeters, J., and Müller, J.-F.: HO_x radical regeneration in isoprene oxidation via peroxy radical
1448 isomerisations. II: experimental evidence and global impact, *Phys. Chem. Chem. Phys.*, 12, 14227-14235,
1449 doi:10.1039/C0CP00811G, 2010.

1450

1451 Peeters, J., Müller, J. F., Stavrou, T., and Vinh Son, N.: Hydroxyl radical recycling in isoprene
1452 oxidation driven by hydrogen bonding and hydrogen tunneling: The upgraded LIM1 mechanism, *J. Phys.*
1453 *Chem. A*, 118, doi:10.1021/jp5033146, 2014.

1454

1455 Praske, E., Crouse, J. D., Bates, K. H., Kurtén, T., Kjaergaard, H. G., and Wennberg, P. O.: Atmospheric
1456 Fate of Methyl Vinyl Ketone: Peroxy Radical Reactions with NO and HO₂, *J. Phys. Chem. A*, 119, 4562-
1457 4572, doi:10.1021/jp5107058, 2015.

1458

1459 Ren, X., Harder, H., Martinez, M., Leshner, R. L., Olinger, A., Simpas, J. B., Brune, W. H., Schwab, J. J.,
1460 Demerjian, K. L., He, Y., Zhou, X., and Gao, H.: OH and HO₂ Chemistry in the urban atmosphere of
1461 New York City, *Atmos. Environ.*, 37, 3639-3651, doi:doi.org/10.1016/S1352-2310(03)00459-X, 2003.

1462

1463 Ren, X., Brune, W. H., Mao, J., Mitchell, M. J., Leshner, R. L., Simpas, J. B., Metcalf, A. R., Schwab, J. J.,
1464 Cai, C., Li, Y., Demerjian, K. L., Felton, H. D., Boynton, G., Adams, A., Perry, J., He, Y., Zhou, X., and
1465 Hou, J.: Behavior of OH and HO₂ in the winter atmosphere in New York City, *Atmos. Environ.*, 40, 252-
1466 263, doi:10.1016/j.atmosenv.2005.11.073, 2006.

1467
1468 Ren, X., van Duin, D., Cazorla, M., Chen, S., Mao, J., Zhang, L., Brune, W. H., Flynn, J. H., Grossberg,
1469 N., Lefer, B. L., Rappenglück, B., Wong, K. W., Tsai, C., Stutz, J., Dibb, J. E., Thomas Jobson, B., Luke,
1470 W. T., and Kelley, P.: Atmospheric oxidation chemistry and ozone production: Results from SHARP
1471 2009 in Houston, Texas, *J. Geophys. Res.: Atmos.*, 118, 5770-5780, doi:10.1002/jgrd.50342, 2013.

1472
1473 Rhew, R. C., Deventer, M. J., Turnipseed, A. A., Warneke, C., Ortega, J., Shen, S., Martinez, L., Koss, A.,
1474 Lerner, B. M., Gilman, J. B., Smith, J. N., Guenther, A. B., and de Gouw, J. A.: Ethene, propene, butene
1475 and isoprene emissions from a ponderosa pine forest measured by relaxed eddy accumulation, *Atmos.*
1476 *Chem. Phys.*, 17, 13417-13438, doi:10.5194/acp-17-13417-2017, 2017.

1477
1478 Rohrer, F., Bohn, B., Brauers, T., Brüning, D., Johnen, F. J., Wahner, A., and Kleffmann, J.:
1479 Characterisation of the photolytic HONO-source in the atmosphere simulation chamber SAPHIR, *Atmos.*
1480 *Chem. Phys.*, 5, 2189-2201, doi:10.5194/acp-5-2189-2005, 2005.

1481
1482 Rohrer, F., Lu, K., Hofzumahaus, A., Bohn, B., Brauers, T., Chang, C.-C., Fuchs, H., Häseler, R.,
1483 Holland, F., Hu, M., Kita, K., Kondo, Y., Li, X., Lou, S., Oebel, A., Shao, M., Zeng, L., Zhu, T., Zhang,
1484 Y., and Wahner, A.: Maximum efficiency in the hydroxyl-radical-based self-cleansing of the troposphere,
1485 *Nat. Geosci.*, 7, 559, doi:10.1038/ngeo2199, 2014.

1486
1487 Rolletter, M., Kaminski, M., Acir, I. H., Bohn, B., Dorn, H. P., Li, X., Lutz, A., Nehr, S., Rohrer, F.,
1488 Tillmann, R., Wegener, R., Hofzumahaus, A., Kiendler-Scharr, A., Wahner, A., and Fuchs, H.:
1489 Investigation of the α -pinene photooxidation by OH in the atmospheric simulation chamber SAPHIR,
1490 *Atmos. Chem. Phys.*, 19, 11635-11649, doi:10.5194/acp-19-11635-2019, 2019.

1491
1492 Rolletter, M., Blocquet, M., Kaminski, M., Bohn, B., Dorn, H. P., Hofzumahaus, A., Holland, F., Li, X.,
1493 Rohrer, F., Tillmann, R., Wegener, R., Kiendler-Scharr, A., Wahner, A., and Fuchs, H.: Photooxidation of
1494 pinonaldehyde at ambient conditions investigated in the atmospheric simulation chamber SAPHIR,
1495 *Atmos. Chem. Phys.*, 20, 13701-13719, doi:10.5194/acp-20-13701-2020, 2020.

1496
1497 Sarkar, C., Guenther, A. B., Park, J. H., Seco, R., Alves, E., Batalha, S., Santana, R., Kim, S., Smith, J.,
1498 Tóta, J., and Vega, O.: PTR-TOF-MS eddy covariance measurements of isoprene and monoterpene fluxes
1499 from an eastern Amazonian rainforest, *Atmos. Chem. Phys.*, 20, 7179-7191, doi:10.5194/acp-20-7179-
1500 2020, 2020.

1501
1502 Sillman, S., Logan, J. A., and Wofsy, S. C.: The sensitivity of ozone to nitrogen oxides and hydrocarbons
1503 in regional ozone episodes, *J. Geophys. Res.: Atmos.*, 95, 1837-1851, doi:10.1029/JD095iD02p01837,
1504 1990.

1505

1506 Slater, E. J., Whalley, L. K., Woodward-Massey, R., Ye, C., Lee, J. D., Squires, F., Hopkins, J. R.,
1507 Dunmore, R. E., Shaw, M., Hamilton, J. F., Lewis, A. C., Crilley, L. R., Kramer, L., Bloss, W., Vu, T.,
1508 Sun, Y., Xu, W., Yue, S., Ren, L., Acton, W. J. F., Hewitt, C. N., Wang, X., Fu, P., and Heard, D. E.:
1509 Elevated levels of OH observed in haze events during wintertime in central Beijing, *Atmos. Chem. Phys.*,
1510 20, 14847-14871, doi:10.5194/acp-20-14847-2020, 2020.

1511
1512 Sommariva, R., Bloss, W. J., Brough, N., Carslaw, N., Flynn, M., Haggerstone, A. L., Heard, D. E.,
1513 Hopkins, J. R., Lee, J. D., Lewis, A. C., McFiggans, G., Monks, P. S., Penkett, S. A., Pilling, M. J., Plane,
1514 J. M. C., Read, K. A., Saiz-Lopez, A., Rickard, A. R., and Williams, P. I.: OH and HO₂ chemistry during
1515 NAMBLEX: roles of oxygenates, halogen oxides and heterogeneous uptake, *Atmos. Chem. Phys.*, 6,
1516 1135-1153, doi:10.5194/acp-6-1135-2006, 2006.

1517
1518 Sommariva, R., Hollis, L. D. J., Sherwen, T., Baker, A. R., Ball, S. M., Bandy, B. J., Bell, T. G.,
1519 Chowdhury, M. N., Cordell, R. L., Evans, M. J., Lee, J. D., Reed, C., Reeves, C. E., Roberts, J. M., Yang,
1520 M., and Monks, P. S.: Seasonal and geographical variability of nitryl chloride and its precursors in
1521 Northern Europe, *Atmos. Sci. Lett.*, 19, e844, doi:10.1002/asl.844, 2018.

1522
1523 Song, H., Chen, X., Lu, K., Zou, Q., Tan, Z., Fuchs, H., Wiedensohler, A., Moon, D. R., Heard, D. E.,
1524 Baeza-Romero, M. T., Zheng, M., Wahner, A., Kiendler-Scharr, A., and Zhang, Y.: Influence of aerosol
1525 copper on HO₂ uptake: a novel parameterized equation, *Atmos. Chem. Phys.*, 20, 15835-15850,
1526 doi:10.5194/acp-20-15835-2020, 2020.

1527
1528 Spirig, C., Neftel, A., Ammann, C., Dommen, J., Grabmer, W., Thielmann, A., Schaub, A., Beauchamp,
1529 J., Wisthaler, A., and Hansel, A.: Eddy covariance flux measurements of biogenic VOCs during ECHO
1530 2003 using proton transfer reaction mass spectrometry, *Atmos. Chem. Phys.*, 5, 465-481,
1531 doi:10.5194/acp-5-465-2005, 2005.

1532
1533 Stone, D., Whalley, L. K., and Heard, D. E.: Tropospheric OH and HO₂ radicals: field measurements and
1534 model comparisons, *Chem. Soc. Rev.*, 41, 6348-6404, doi:10.1039/C2CS35140D, 2012.

1535
1536 Stone, D., Sherwen, T., Evans, M. J., Vaughan, S., Ingham, T., Whalley, L. K., Edwards, P. M., Read, K.
1537 A., Lee, J. D., Moller, S. J., Carpenter, L. J., Lewis, A. C., and Heard, D. E.: Impacts of bromine and
1538 iodine chemistry on tropospheric OH and HO₂: comparing observations with box and global model
1539 perspectives, *Atmos. Chem. Phys.*, 18, 3541-3561, doi:10.5194/acp-18-3541-2018, 2018.

1540
1541 Taketani, F., Kanaya, Y., and Akimoto, H.: Kinetics of Heterogeneous Reactions of HO₂ Radical at
1542 Ambient Concentration Levels with (NH₄)₂SO₄ and NaCl Aerosol Particles, *J. Phys. Chem. A*, 112,
1543 2370-2377, doi:10.1021/jp0769936, 2008.

1544
1545 Taketani, F., Kanaya, Y., and Akimoto, H.: Heterogeneous loss of HO₂ by KCl, synthetic sea salt, and
1546 natural seawater aerosol particles, *Atmos. Environ.*, 43, 1660-1665, doi:10.1016/j.atmosenv.2008.12.010,
1547 2009.

1548

1549 Tan, D., Faloon, I., Simpas, J. B., Brune, W., Shepson, P. B., Couch, T. L., Sumner, A. L., Carroll, M.
1550 A., Thornberry, T., Apel, E., Riemer, D., and Stockwell, W.: HO_x budgets in a deciduous forest: Results
1551 from the PROPHET summer 1998 campaign, *J. Geophys. Res.: Atmos.*, 106, 24407-24427,
1552 doi:10.1029/2001jd900016, 2001.

1553
1554 Tan, Z., Fuchs, H., Lu, K., Hofzumahaus, A., Bohn, B., Broch, S., Dong, H., Gomm, S., Häsel, R., He,
1555 L., Holland, F., Li, X., Liu, Y., Lu, S., Rohrer, F., Shao, M., Wang, B., Wang, M., Wu, Y., Zeng, L.,
1556 Zhang, Y., Wahner, A., and Zhang, Y.: Radical chemistry at a rural site (Wangdu) in the North China
1557 Plain: observation and model calculations of OH, HO₂ and RO₂ radicals, *Atmos. Chem. Phys.*, 17, 663-
1558 690, doi:10.5194/acp-17-663-2017, 2017.

1559
1560 Tan, Z., Rohrer, F., Lu, K., Ma, X., Bohn, B., Broch, S., Dong, H., Fuchs, H., Gkatzelis, G. I.,
1561 Hofzumahaus, A., Holland, F., Li, X., Liu, Y., Liu, Y., Novelli, A., Shao, M., Wang, H., Wu, Y., Zeng, L.,
1562 Hu, M., Kiendler-Scharr, A., Wahner, A., and Zhang, Y.: Wintertime photochemistry in Beijing:
1563 observations of RO_x radical concentrations in the North China Plain during the BEST-ONE campaign,
1564 *Atmos. Chem. Phys.*, 18, 12391-12411, doi:10.5194/acp-18-12391-2018, 2018.

1565
1566 Tan, Z., Lu, K., Hofzumahaus, A., Fuchs, H., Bohn, B., Holland, F., Liu, Y., Rohrer, F., Shao, M., Sun,
1567 K., Wu, Y., Zeng, L., Zhang, Y., Zou, Q., Kiendler-Scharr, A., Wahner, A., and Zhang, Y.: Experimental
1568 budgets of OH, HO₂, and RO₂ radicals and implications for ozone formation in the Pearl River Delta in
1569 China 2014, *Atmos. Chem. Phys.*, 19, 7129-7150, doi:10.5194/acp-19-7129-2019, 2019.

1570
1571 Tan, Z., Hofzumahaus, A., Lu, K., Brown, S. S., Holland, F., Huey, L. G., Kiendler-Scharr, A., Li, X.,
1572 Liu, X., Ma, N., Min, K.-E., Rohrer, F., Shao, M., Wahner, A., Wang, Y., Wiedensohler, A., Wu, Y., Wu,
1573 Z., Zeng, L., Zhang, Y., and Fuchs, H.: No Evidence for a Significant Impact of Heterogeneous
1574 Chemistry on Radical Concentrations in the North China Plain in Summer 2014, *Environ. Sci. Technol.*,
1575 54, 5973-5979, doi:10.1021/acs.est.0c00525, 2020.

1576
1577 Tan, Z., Fuchs, H., Hofzumahaus, A., Bloss, W. J., Bohn, B., Cho, C., Hohaus, T., Holland, F.,
1578 Lakshmisha, C., Liu, L., Monks, P. S., Novelli, A., Niether, D., Rohrer, F., Tillmann, R., Valkenburg, T.,
1579 Vardhan, V., Kiendler-Scharr, A., Wahner, A., and Sommariva, R.: Seasonal variation of nitryl chloride
1580 and its relation to gas-phase precursors during the JULIAC campaign in Germany, *Atmos. Chem. Phys.*
1581 *Discuss.*, 2022, 1-30, doi:10.5194/acp-2022-386, 2022.

1582
1583 Tanaka, P. L., Riemer, D. D., Chang, S., Yarwood, G., McDonald-Buller, E. C., Apel, E. C., Orlando, J. J.,
1584 Silva, P. J., Jimenez, J. L., Canagaratna, M. R., Neece, J. D., Mullins, C. B., and Allen, D. T.: Direct
1585 evidence for chlorine-enhanced urban ozone formation in Houston, Texas, *Atmos. Environ.*, 37, 1393-
1586 1400, doi:10.1016/S1352-2310(02)01007-5, 2003.

1587
1588 Teng, A. P., Crouse, J. D., and Wennberg, P. O.: Isoprene peroxy radical dynamics, *J. Am. Chem. Soc.*,
1589 139, 5367-5377, doi:10.1021/jacs.6b12838, 2017.

1590
1591 Thornton, J. A., Kercher, J. P., Riedel, T. P., Wagner, N. L., Cozic, J., Holloway, J. S., Dubé, W. P.,
1592 Wolfe, G. M., Quinn, P. K., Middlebrook, A. M., Alexander, B., and Brown, S. S.: A large atomic

1593 chlorine source inferred from mid-continental reactive nitrogen chemistry, *Nature*, 464, 271-274,
1594 doi:10.1038/nature08905, 2010.

1595
1596 Vaughan, S., Ingham, T., Whalley, L. K., Stone, D., Evans, M. J., Read, K. A., Lee, J. D., Moller, S. J.,
1597 Carpenter, L. J., Lewis, A. C., Fleming, Z. L., and Heard, D. E.: Seasonal observations of OH and HO₂ in
1598 the remote tropical marine boundary layer, *Atmos. Chem. Phys.*, 12, 2149-2172, doi:10.5194/acp-12-
1599 2149-2012, 2012.

1600
1601 Vilà-Guerau de Arellano, J., van den Dries, K., and Pino, D.: On inferring isoprene emission surface flux
1602 from atmospheric boundary layer concentration measurements, *Atmos. Chem. Phys.*, 9, 3629-3640,
1603 doi:10.5194/acp-9-3629-2009, 2009.

1604
1605 Wang, F., Hu, R., Chen, H., Xie, P., Wang, Y., Li, Z., Jin, H., Liu, J., and Liu, W.: Development of a field
1606 system for measurement of tropospheric OH radical using laser-induced fluorescence technique, *Optics*
1607 *Express*, 27, A419-A435, doi:10.1364/OE.27.00A419, 2019.

1608
1609 Whalley, L. K., Edwards, P. M., Furneaux, K. L., Goddard, A., Ingham, T., Evans, M. J., Stone, D.,
1610 Hopkins, J. R., Jones, C. E., Karunaharan, A., Lee, J. D., Lewis, A. C., Monks, P. S., Moller, S. J., and
1611 Heard, D. E.: Quantifying the magnitude of a missing hydroxyl radical source in a tropical rainforest,
1612 *Atmos. Chem. Phys.*, 11, 7223-7233, doi:10.5194/acp-11-7223-2011, 2011.

1613
1614 Whalley, L. K., Stone, D., Dunmore, R., Hamilton, J., Hopkins, J. R., Lee, J. D., Lewis, A. C., Williams,
1615 P., Kleffmann, J., Laufs, S., Woodward-Massey, R., and Heard, D. E.: Understanding in situ ozone
1616 production in the summertime through radical observations and modelling studies during the Clean air for
1617 London project (ClearfLo), *Atmos. Chem. Phys.*, 18, 2547-2571, doi:10.5194/acp-18-2547-2018, 2018.

1618
1619 Whalley, L. K., Slater, E. J., Woodward-Massey, R., Ye, C., Lee, J. D., Squires, F., Hopkins, J. R.,
1620 Dunmore, R. E., Shaw, M., Hamilton, J. F., Lewis, A. C., Mehra, A., Worrall, S. D., Bacak, A., Bannan,
1621 T. J., Coe, H., Percival, C. J., Ouyang, B., Jones, R. L., Crilley, L. R., Kramer, L. J., Bloss, W. J., Vu, T.,
1622 Kotthaus, S., Grimmond, S., Sun, Y., Xu, W., Yue, S., Ren, L., Acton, W. J. F., Hewitt, C. N., Wang, X.,
1623 Fu, P., and Heard, D. E.: Evaluating the sensitivity of radical chemistry and ozone formation to ambient
1624 VOCs and NO_x in Beijing, *Atmos. Chem. Phys.*, 21, 2125-2147, doi:10.5194/acp-21-2125-2021, 2021.

1625
1626 Winiberg, F. A. F., Dillon, T. J., Orr, S. C., Groß, C. B. M., Bejan, I., Brumby, C. A., Evans, M. J., Smith,
1627 S. C., Heard, D. E., and Seakins, P. W.: Direct measurements of OH and other product yields from the
1628 HO₂ + CH₃C(O)O₂ reaction, *Atmos. Chem. Phys.*, 16, 4023-4042, doi:10.5194/acp-16-4023-2016, 2016.

1629
1630 Wolfe, G. M., Thornton, J. A., Bouvier-Brown, N. C., Goldstein, A. H., Park, J. H., McKay, M., Matross,
1631 D. M., Mao, J., Brune, W. H., LaFranchi, B. W., Browne, E. C., Min, K. E., Wooldridge, P. J., Cohen, R.
1632 C., Crouse, J. D., Faloona, I. C., Gilman, J. B., Kuster, W. C., de Gouw, J. A., Huisman, A., and Keutsch,
1633 F. N.: The Chemistry of Atmosphere-Forest Exchange (CAFE) Model – Part 2: Application to
1634 BEARPEX-2007 observations, *Atmos. Chem. Phys.*, 11, 1269-1294, doi:10.5194/acp-11-1269-2011,
1635 2011.

1636

1637 Wolfe, G. M., Cantrell, C., Kim, S., Mauldin Iii, R. L., Karl, T., Harley, P., Turnipseed, A., Zheng, W.,
1638 Flocke, F., Apel, E. C., Hornbrook, R. S., Hall, S. R., Ullmann, K., Henry, S. B., DiGangi, J. P., Boyle, E.
1639 S., Kaser, L., Schnitzhofer, R., Hansel, A., Graus, M., Nakashima, Y., Kajii, Y., Guenther, A., and
1640 Keutsch, F. N.: Missing peroxy radical sources within a summertime ponderosa pine forest, *Atmos. Chem.*
1641 *Phys.*, 14, 4715-4732, doi:10.5194/acp-14-4715-2014, 2014.

1642

1643